DESIGN OF V-BAND SUBSTRATE INTEGRATED WAVEGUIDE FED APERTURE COUPLED MICROSTRIP PATCH ARRAYS WITH CIRCULAR POLARIZATION AND PARASITIC PATCH FOR OFF-BODY COMMUNICATIONS IN BODY CENTRIC WIRELESS NETWORKS. By:

Rubén F.M Delgado Castillo

A Thesis Submitted in Partial Fulfillment of the Requirements for the Degree of:

MASTER OF SCIENCE

In

Electrical Engineering

UNIVERSITY OF PUERTO RICO
MAYAGUEZ CAMPUS

May 2017,

Approved By:

_____	_____
Rocio Zapata, Profa. Representative, Graduate School	Date
_____	_____
José G. Colom-Ustariz, Ph.D Member, Graduate Committee	Date
_____	_____
Rafael Medina, Ph.D Member, Graduate Committee	Date
_____	_____
Rafael Rodríguez Solís, Ph.D President, Graduate Comittee	Date
_____	_____
José G. Colom-Ustariz, Ph.D Interim Associate Director, Electrical and Computer Engineer Department	Date

Abstract of Thesis Presented to the Graduate School
of the University of Puerto Rico in Partial Fulfillment of the
Requirements for the Degree of Master of Science

DESIGN OF V-BAND SUBSTRATE INTEGRATED WAVEGUIDE FED APERTURE COUPLED MICROSTRIP PATCH ARRAYS WITH CIRCULAR POLARIZATION AND PARASITIC PATCH FOR OFF-BODY COMMUNICATIONS IN BODY CENTRIC WIRELESS NETWORKS

By

Rubén F. M Delgado Castillo

May 2017

Chair: Rafael A. Rodríguez Solís

Mayor Department: Electrical and Computer Engineering

This work presents the design of a multi-layer radiating element and a multi-layer 2x2 array for use in 60 GHz body centric wireless networks. The antenna designed operates with an impedance bandwidth of 11.6%, from 57 to 64 GHz, covering the IEEE 802.11ad standard. The antenna element has a circularly polarized radiation, with a 9.2% axial ratio bandwidth. The antenna gain is 7.06 dBc circular gain at the central frequency.

The antenna element is fed through a taper in substrate integrated waveguide (SIW), and a coaxial to SIW transition. A SIW tapered line helps to increase the impedance from the coaxial to the antenna impedance. SIW lines were designed in two layers to reduce the substrate size of the feed. The first feed layer contain SIW taper line, and in the second the coaxial transition. The coaxial transition work as individual design that can be implemented in another designs and in the 2x2 array.

The effect of the human body on the electric parameters of the antennas at 60 GHz was studied. The presence of skin has a negligible effect on electrical performance of the antennas at the frequency of interest.

Resumen de Tesis Presentado a Escuela Graduada
De la Universidad de Puerto Rico como requisito parcial de los
Requerimientos para el grado de Maestría en Ciencias

DISEÑO DE ARREGLO DE PARCHO BANDA-V ACOPLADO POR APERTURA Y ALIMENTADO POR GUIA DE ONDA INTEGRADA EN EL SUSTRATO CON POLARIZACION CIRCULAR Y PARASITICO PARA COMUNICACION INALAMBRICA CENTRADA EN EL CUERPO HACIA FUERA DEL CUERPO.

Por

Rubén F. M Delgado Castillo

Mayo 2017

Consejero: Rafael A. Rodríguez Solís

Departamento: Ingeniería Eléctrica y de Computadoras

Este trabajo presenta el diseño de un elemento de radiación con múltiples capas y un arreglo 2x2 que opera a 60 GHz para redes inalámbricas centradas en el cuerpo. El diseño de antena opera con una banda de impedancia de 11.6%, desde 57 to 64 GHz, cubriendo el estándar de IEEE 802.11ad. El elemento de antena tiene un patrón de radiación de polarización circular con un 9.2% banda de relación axial. La antena tiene 7.06 dBc de ganancia circular en la frecuencia central.

El elemento de antena fue alimentado atreves de una reducción gradual en guía de onda integrada en el substrato (SIW). La línea con reducción gradual en SIW ayuda a incrementar la impedancia del coaxial a la impedancia de la antena. La línea en SIW fue diseñada en dos capas para reducir el tamaño del sustrato para el alimentador. La primera capa del alimentador contiene la línea de reducción gradual en SIW y la segunda contiene la transición de coaxial. La transición de coaxial trabaja como un diseño individual que puede ser implementado en otros diseños y en el arreglo 2x2.

Los efectos del cuerpo humano en los parámetros eléctricos de la antena a 60 GHz fueron estudiados. La presencia de piel tiene un efecto insignificante en el funcionamiento de la antena en la frecuencia de interés.

TABLE OF CONTENTS

LIST OF TABLES

LIST OF FIGURES

CHAPTER 1

INTRODUCTION

Microstrip patch antennas are simple, low profile, light weight, and can be made conformal to the body's surface in Body-Centric Wireless Communications Systems (BWCS). Since they have low back radiation, microstrip antennas are an attractive solutions for off-body communications in BWCS. At 60 GHz, off-body communication antennas can be integrated directly to clothing, or placed directly on the skin, and because the low power requirements, there is no expected harm to the tissue below. At 60 GHz, there are high losses due to atmospheric absorption, providing an additional layer of security in body centric systems. Also, interactions with the human body at V-band occur mostly at the skin outmost layers, having negligible effect on the antenna's electrical performance, for example in gain, input impedance, and efficiency [1].

Transmission and reception antennas are placed at close proximity at 60 GHz, because of the atmospheric absorption at 10 m using 60 GHz is about 2 dB [1]. Using V-band, allows the system to provide high capacity data transfer in medical, military or civilian applications. Also, using circular polarization can provide a more stable communication channel for the data transfer, as circular polarized antennas suffer less signal loss due to polarization mismatch than linearly polarized antennas.

1.1 Objectives

The goal of this work is to design an antenna to be used for off-body communications in BANs. The antenna will be designed to operate in V-band, allowing high capacity data transfer in medical, military or civilian applications. The bandwidth requirement for the antenna is the Federal Communications Commission (FCC) 13-112. The design goal is to provide a circular polarized single element with a large axial ratio bandwidth that can cover most of the IEEE 802.11ad band, with good gain and large impedance bandwidth. The

element design needs to be easily integrated into an array to increase the gain and axial ratio bandwidth. The array antenna goal is to improve the axial ratio to cover the band of interest, as well as the impedance bandwidth with a good circular polarization gain.

1.2 Work Organization

This work is organized into 3 main sections. Chapter 2 presents a literature review which discusses previous work at 60 GHz, antennas for body area networks, high gain patch antennas, and circular polarization method and benefits. Chapter 3 presents the methodology and the antennas considered for off-body communications applications. Chapter 4 presents the results for the final single element. Chapter 5 presents conclusions and recommendations for future work.

CHAPTER 2

LITERATURE REVIEW AND BACKGROUND

2.1 Antenna for off-body communications

Antennas for Body-Centric Wireless Systems (BWCS) have been studied on [1] considering electrical properties over a phantom at millimeter-wave frequencies. Antennas are the key point for satisfactory power transfer between nodes placed on different parts of the human body for communications with on- and off-body devices. In [2], on-body communications at 60 GHz using a skin-equivalent semisolid phantom is considered. The phantom was designed and fabricated to emulate the permittivity values of human skin in the presence of an antenna. In [3], the approach is to perform a Design of Experiments for off-body communications at 60 GHz. A homogeneous skin model was designed to simulate human skin in HFSS. The data for the model was obtained from [4] for dry skin. Table 2.1. (taken from [4]) shows the electric properties for dry skin. The authors in [3] showed that the antenna electrical properties were not affected by the skin presence.

TABLE 2.1. Electric Properties of Skin [5].

Tissue name	Frequency [GHz]	Conductivity [S/m]	Relative permittivity	Loss tangent	Wavelength [mm]	Penetration depth [mm]
Dry Skin	50	34.619	9.4021	1.3237	1.6959	5.4216
	52	35.04	9.0634	1.3364	1.6577	5.2692
	54	35.424	8.7544	1.347	1.6216	5.1305
	56	35.777	8.4718	1.3556	1.5876	5.0037
	58	36.1	8.2129	1.3623	1.5552	4.8875
	60	36.397	7.9753	1.3673	1.5245	4.7805
	62	36.671	7.7567	1.3707	1.4952	4.6817
	64	36.925	7.5554	1.3727	1.4672	4.5902
	66	37.159	7.3695	1.3733	1.4404	4.5052
	68	37.376	7.1976	1.3727	1.4148	4.4262
	70	37.577	7.0383	1.371	1.3902	4.3524

2.2 Circular Polarization Antenna

Circular polarization (CP) antennas suffer less loss due to polarization mismatch, than linearly polarized ones [5], which is good for off-body communications data transfer. The CP antennas can be obtained using single feed points and multiple feed points on microstrip patches. Multiple feed points can achieve better axial ratio (AR) bandwidth than single feeds. Configurations for CP using microstrip patch antennas can be obtained with standard geometries, as demonstrated in [6] for single and multiple feed points. Fig. 2.1. shows some methods to achieve CP in microstrip patch antennas. However, in [7] it is shown a microstrip patch rotated 45° with respect of the slot aperture feed, achieving more than 2% axial ratio bandwidth using double resonance with the slot aperture. On the other hand, the work in [8] obtains a 35% AR bandwidth using dual capacitive coupled feeds.

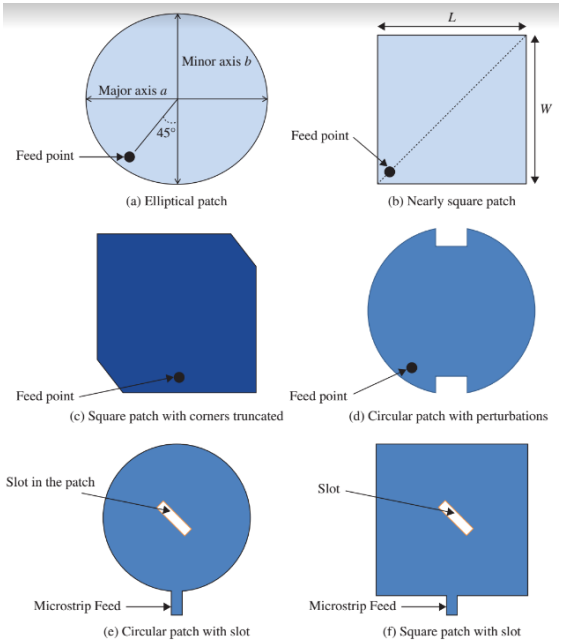

Fig. 2.1. Circular and square patches with CP using single feed point [7].

2.3 Sequentially Rotated Array Antennas

Antenna arrays with phase arrangements techniques generate circular polarization pattern with axial ratio bandwidths greater than 10%. Phase arrangements, as shown in [9] can be implemented for different type of antennas. Huang shows in [9] different phase arrangements using rectangular patches, and dipoles using only one feed in each patch. The feed phases for each element in the array are $0°, 90°, 0°, 90°$ or $0°, 90°, 180°, 270°$ as shown in Fig. 2.2. In [9] the phase difference is implemented with phase shifters, but at 60 GHz for BANs it would not be practical, since they are expensive. Also, to reduce cost it is recommended using the $0°, 90°, 0°, 90°$ arrangement, because only one $90°$ hybrid is required.

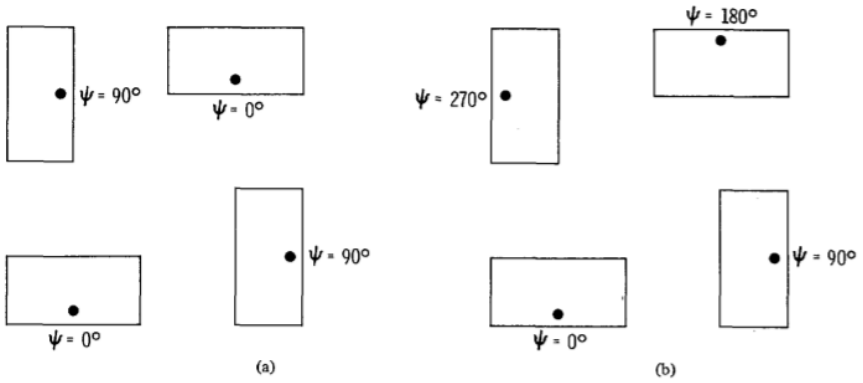

a) $0°, 90°, 0°, 90°$ arrangement b) $0°, 90°, 0°, 90°$ arrangement

Fig. 2.2. 2x2 microstrip array using linear polarized elements [9].

2.4 High Gain Patch Antennas

A simple method to increase antenna gain is using more elements in an array antenna. However, to achieve more gain without increasing the number of elements in a microstrip patch array can be troublesome. One way to accomplish high gain is using parasitic patches. In [10], the use of a parasitic patch provides an additional resonance within the band, increasing the impedance bandwidth. The separation between the fed and parasitic patches can also be used to increase the gain. In [11] it is shown that changing the distance between patches can increase impedance bandwidth or the total gain. In other words, the designer needs to choose the substrate thickness to improve the impedance bandwidth or the total gain,

or to have a compromise between them. Table 2.2. (taken from [11]) shows the results for the impedance bandwidth and the total gain when is changed the air gap between both patches is changed. The antenna design from [11] is a two microstrip square patches on top of substrates with air gap between two substrates feed with a coaxial cable. The substrates has a permittivity of $\epsilon_r = 2.22$ with a height of 0.159 cm. Both patches measure 2.5 cm and covers the frequency band of 3.7 GHz to 4.2 GHz of the C-band satellite communication. The Δ represent the air gap between the substrates, x, represents the distance of the feed point from the center of the lower patch.

TABLE 2.2. Effect of the Air Gap Δ Between Both Patches [11].

$\Delta(cm)$	$x(cm)$	$f_0(GHz)$	$BW(MHz)$	$Gain(dB)$
0.5	1.10	3.885	684	8.0
1.0	0.60	3.930	167	7.8
1.5	0.40	3.878	85	6.3
2.0	0.35	3.844	58	5.3
2.5	0.30	3.821	45	5.5
3.0	0.30	3.802	39	7.2
3.5	0.30	3.785	41	9.2
4.0	0.35	3.772	54	10.6
4.5	0.40	3.765	85	10.6
5.0	0.50	3.787	134	9.3
5.5	0.50	3.804	132	7.4
6.0	0.50	3.810	108	5.9

2.4 Proposed Antenna Design

The goal of this work is to design an antenna to be used for off-body communications in BWCS. The main goal is to achieve circular polarization using a single feed point. Also, the antenna should cover the entire IEEE 802.11ad frequency band in terms of impedance and axial ratio. The axial ratio bandwidth for the array will be increased using the sequentially rotated method. Furthermore, the array will have higher gain using a circularly polarized element with parasitic patches with increased circular polarization gain.

CHAPTER 3

METHODOLOGY

3.1 Antenna Structure using IEEE 802.11ad Standard

3.1.1 Antenna's Desired Operation

The first antenna is proposed to operate in the 56.16 GHz to 64.8 GHz band, as specified by IEEE 802.11ad standard. All the configurations are designed using Ansys High Frequency Structure Simulator (HFSS) electromagnetic CAD. The antenna must be circularly polarized with wideband axial ratio and impedance bandwidth. The antenna is designed using SIW technology to reduce the front-to-back ratio for off-body communications in BANs. Furthermore, the antenna proposed will have higher gain than conventional patches, to reduce the number of elements on an array.

3.1.2 Single Radiating Element

The initial design for the SIW-fed cavity-backed aperture coupled antenna is based on the work in [12]. The design in [12] was chosen as a starting point due to their wideband impedance bandwidth, and the feed method used to reduce the skin effect on the antenna in BAN applications. The single element impedance bandwidth in [12] was 14.29% from 56.16 GHz to 64.8 GHz. The antenna achieved a broadside gain of 5.58 dBi. The design in [12] was modified to produce circular polarization and to increase the gain by changing the top substrate height. The substrate shared by both patches is Rogers RO 5880 ($\varepsilon_r = 2.2$), instead of air, to reduce the total physical height for maximum gain Fig. 3.1.2.1 shows the antenna model and the design parameters for the circularly polarized patch.

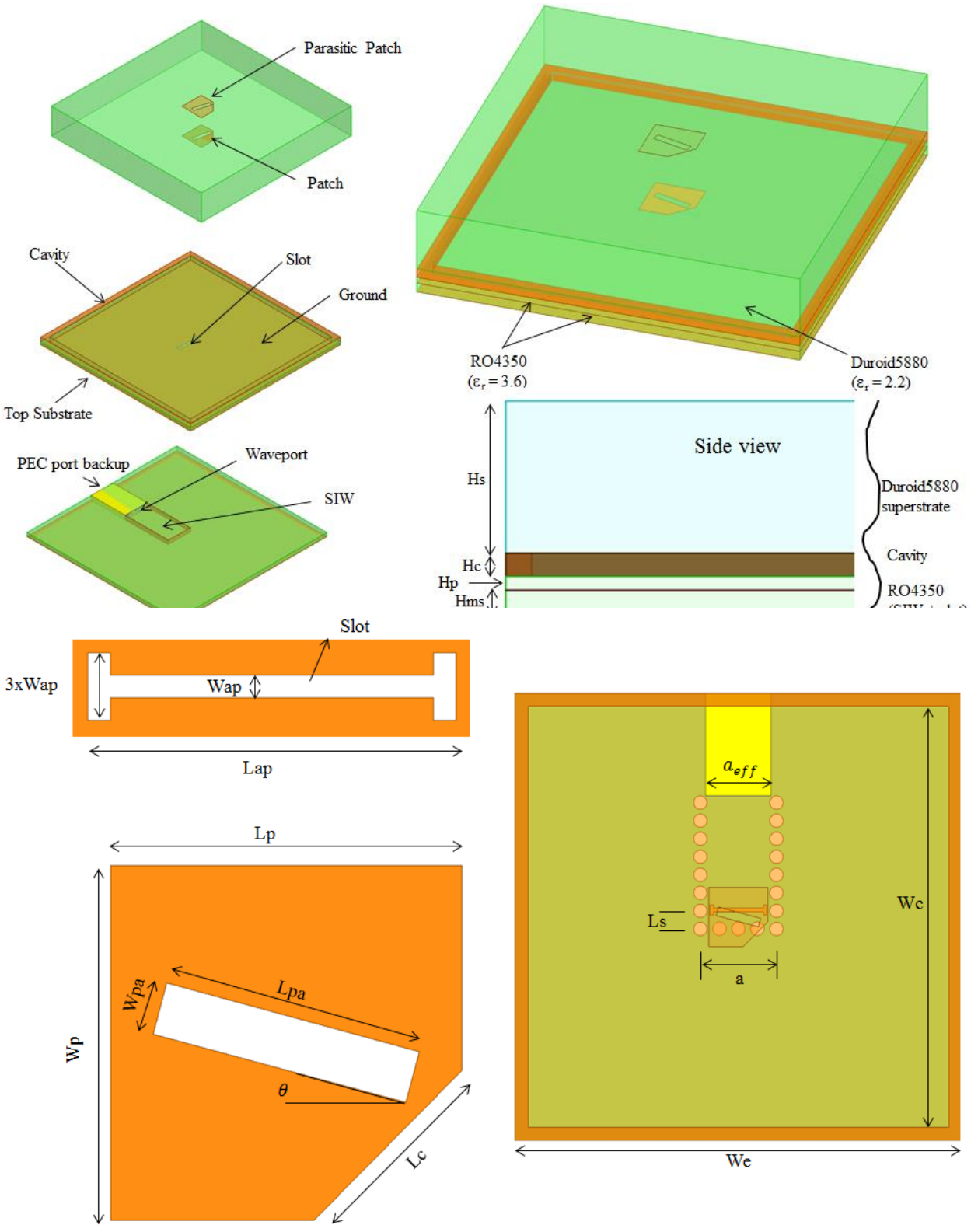

Fig. 3.1.2.1. Antenna geometry and design parameters. The design parameters are summarized in Table 3.1.2.1.

The feeds used in the models shown Fig. 3.1.2.1 were dielectric-filled waveguide, and SIW. The SIW via hole radius, r, is 0.15 mm, the distance between vias, p, is 0.403 mm, and the SIW width, a, is 1.705 mm. The SIW feed design follows [12], which relates the SIW dimensions with the width of a dielectric-filled rectangular waveguide of width a_{eff} [13],

$$a_{eff} = a - \frac{4r^2}{0.95p} \qquad (1)$$

where, a_{eff} is the rectangular waveguide feed width, a, is the SIW width, r, is the radius of the vias, and p, is the distance between vias.

Circular polarization with a single feed point can be achieved using different methods, as discussed in [5]. However, these methods produce narrowband axial ratio (AR) bandwidth. Because of the limited AR bandwidth these methods, the proposed antenna element combines two different methods to improve the axial ratio; truncating one corner of the patch and introducing a diagonal slot on the patch. The dimensions of the truncated corner are initially found through the following equation,

$$d = \frac{\sqrt{w_p^2 + L_p^2}}{2} - L_c \qquad (2)$$

where, d, is the distance between the middle of the patch to the center of the corner cut, W_p and L_p are the patch width and length, respectively, and L_c is the cut distance perpendicular to the cut.

The conventional placing of the slot is centered at the patch center, and rotated 45° from the horizontal. By varying the rotation of the slot in the truncated patch, it is possible to increase the AR bandwidth for the element. The proposed antenna has an improved AR bandwidth by rotating the slot only 15° from the horizontal. Both the fed and parasitic patches modified by the corner truncation and addition of the slot, to increase the AR bandwidth, as well as the gain for the antenna element.

The antenna is fed through aperture coupling. The coupling aperture is a resonant H-slot to help improve the impedance bandwidth. The H-slot aperture was kept smaller than the

patch width to maintain its the radiation completely under the patch. The position of the H-slot aperture is selected to improve the impedance matching, as well as the AR bandwidth. The patches are about 2% smaller than the patches in [12], to move the impedance bandwidth to better comply with the IEEE 802.11ad frequency band. The cavity size was not changed. Table 3.1.2.1 shows the parameters and values for the design from Fig. 3.1.2.1.

TABLE 3.1.2.1. SIW Fed ACMPA Radiating Element Parameters.

Parameter	Value	Parameter	Value
H_s	1.7mm	L_{pa}	0.98mm
H_c	0.254mm	θ	15°
H_p	0.168mm	L_c	0.784mm
H_{ms}	0.254mm	a_{eff}	1.47mm
W_{ap}	0.0784mm	a	1.705mm
L_{ap}	1.274mm	L_s	0.419mm
L_p	1.317mm	W_c	9.6mm
W_p	1.317mm	W_e	10mm
W_{pa}	0.196mm		

Fig. 3.1.2.2 shows the reflection coefficient for the antenna fed through SIW (blue curve) and through an equivalent dielectric-filled waveguide (red curve). The antenna was simulated with a SIW feed and with an equivalent dielectric-filled waveguide feed for two reasons. First, the dielectric-filled waveguide model is much simpler to generate and the simulations run significantly faster when the antenna is fed through a dielectric-filled waveguide, providing a quick way to verify the antenna performance. In addition, since the dielectric-filled waveguide has very low losses, simulating both feeding techniques help to quantify the energy loss in the SIW feed. The antenna has an impedance bandwidth that covers almost the entire IEEE 802.11ad frequency band. The single element impedance is 140Ω at the port, and the reflection coefficient is less than -10 dB from 55.3 GHz to 62.8 GHz. Furthermore, the axial ratio (AR) bandwidth is shown in Fig. 3.1.2.3. and goes from

58.2 GHz to 62.7 GHz (7.8%) which is greater than the 2% found in most cases [5]. Fig. 3.1.2.4. shows the AR at 60 GHz as a function of theta, to determine the feasibility of this element to be used in beam-scanning applications. Note that the AR is less than 3 dB from −19° to 24°. The element has a LHCP gain of 7 dB and a wide beamwidth at 60 GHz (66°), as shown in Fig. 3.1.2.5. Fig. 3.1.2.6. shows the CP gain as a function of frequency. Note that the gain increases from 1.61 dBc at 56.16 GHz to 7.72 dBc at 64 GHz, the gain increases as frequency is increases. The CP gain at the central frequency of 60 GHz is 7.1 dBc. The radiation pattern for the radiating element is shown in Fig. 3.1.2.7. The results for the single radiating element are summarized in Table 3.1.2.2.

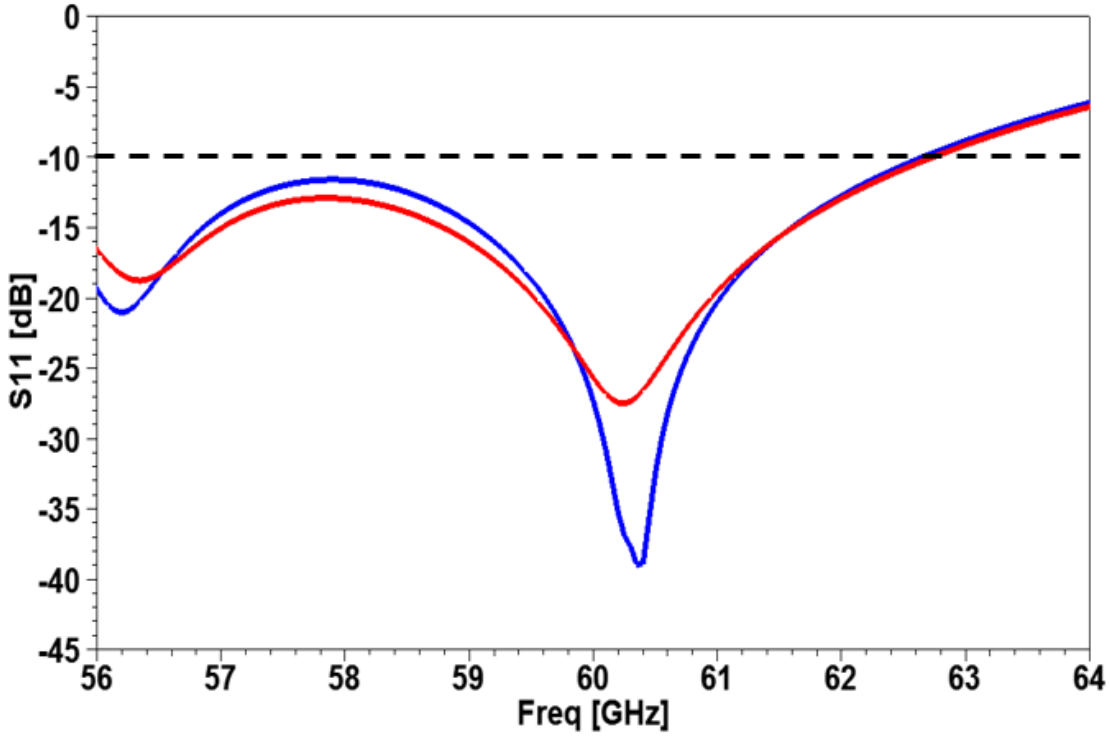

Fig. 3.1.2.2. Reflection coefficient for a single element fed with a dielectric-filled waveguide (red) and with SIW (blue).

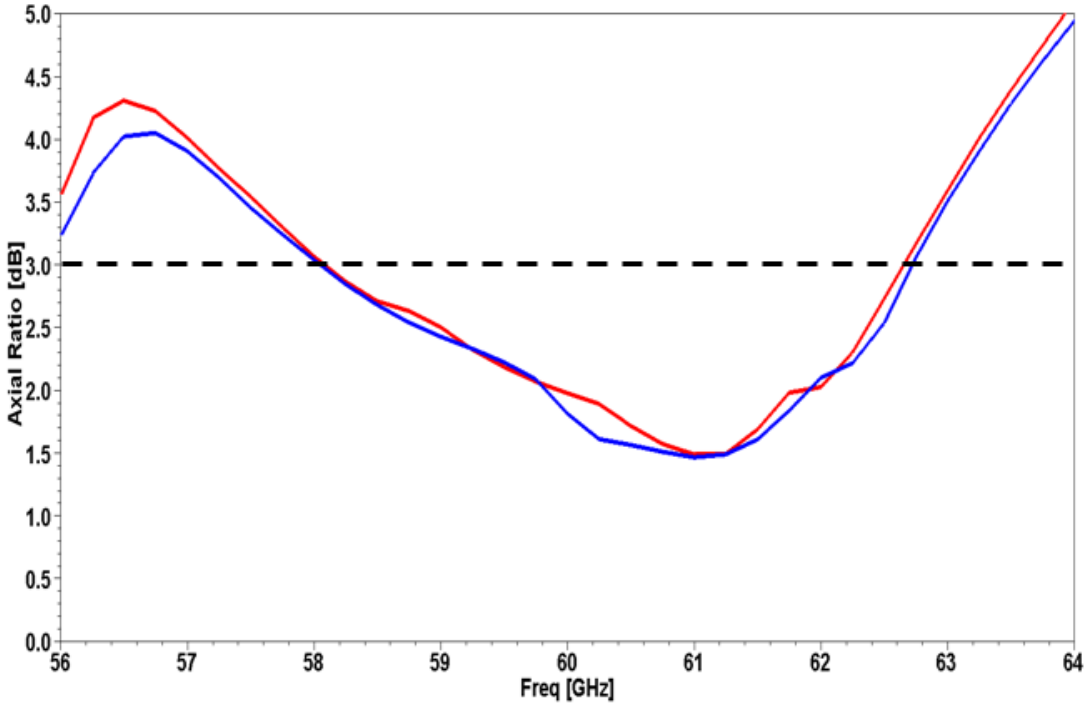

Fig. 3.1.2.3. Axial ratio bandwidth for a single element fed with a dielectric-filled waveguide (red) and with SIW (blue).

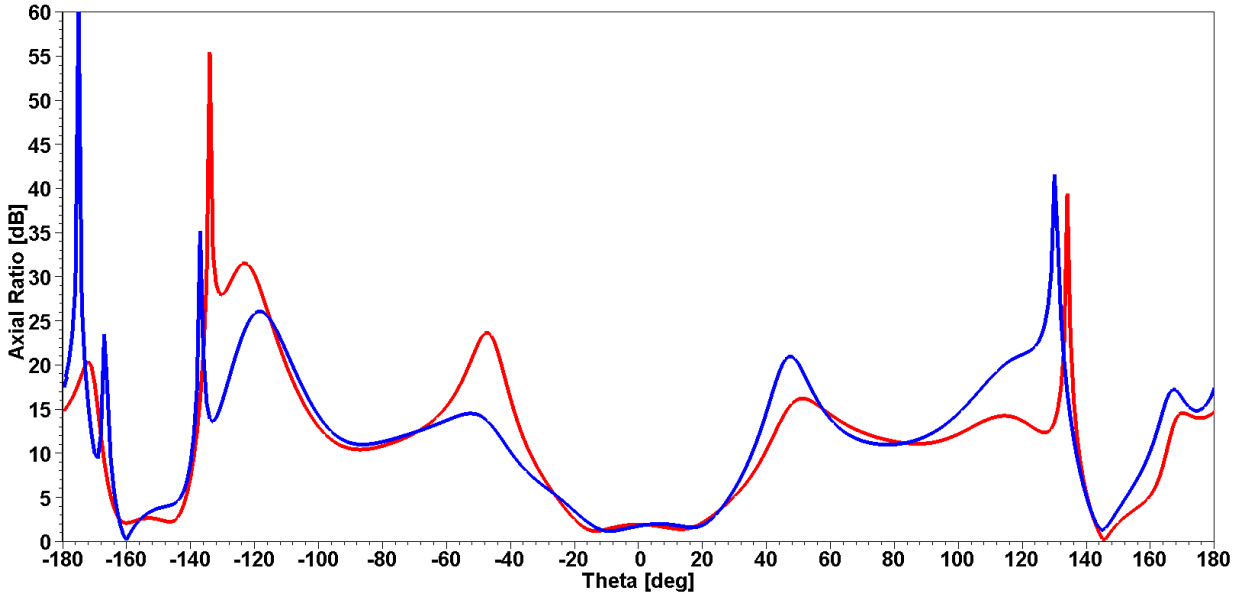

Fig. 3.1.2.4. Axial ratio as a function of theta at 60 GHz for a single element fed with a dielectric-filled waveguide (red) and with SIW (blue).

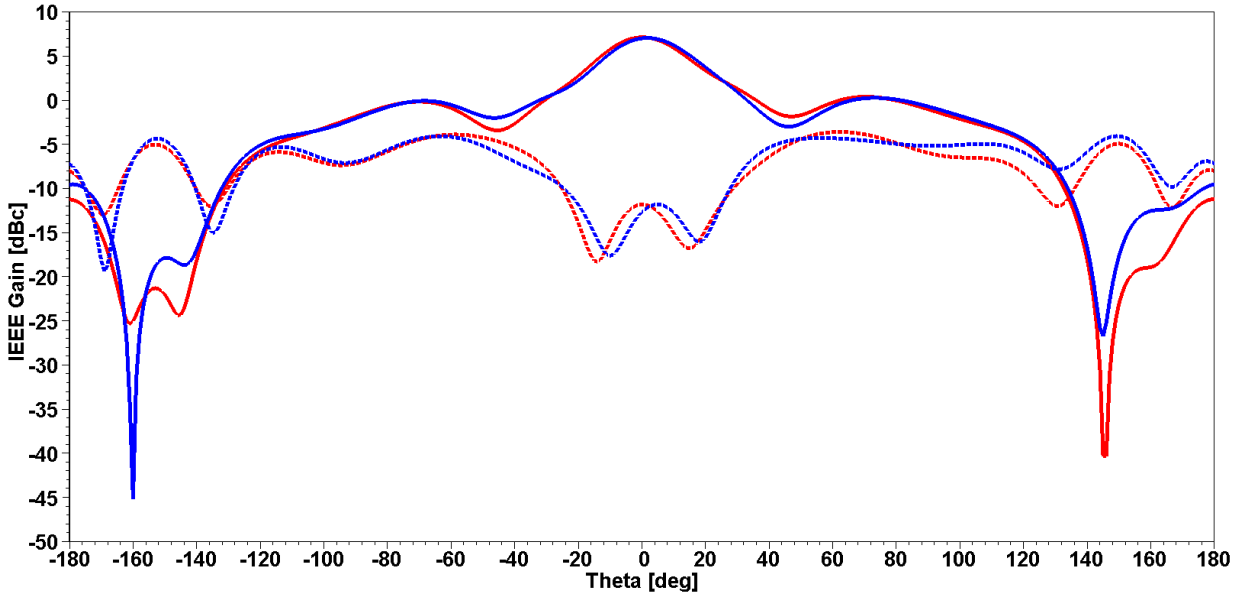

Fig. 3.1.2.5. CP gain pattern for a single element at 60 GHz fed with a dielectric-filled waveguide (red) and with SIW (blue). The dotted line show the cross-polarized gain for the same cases.

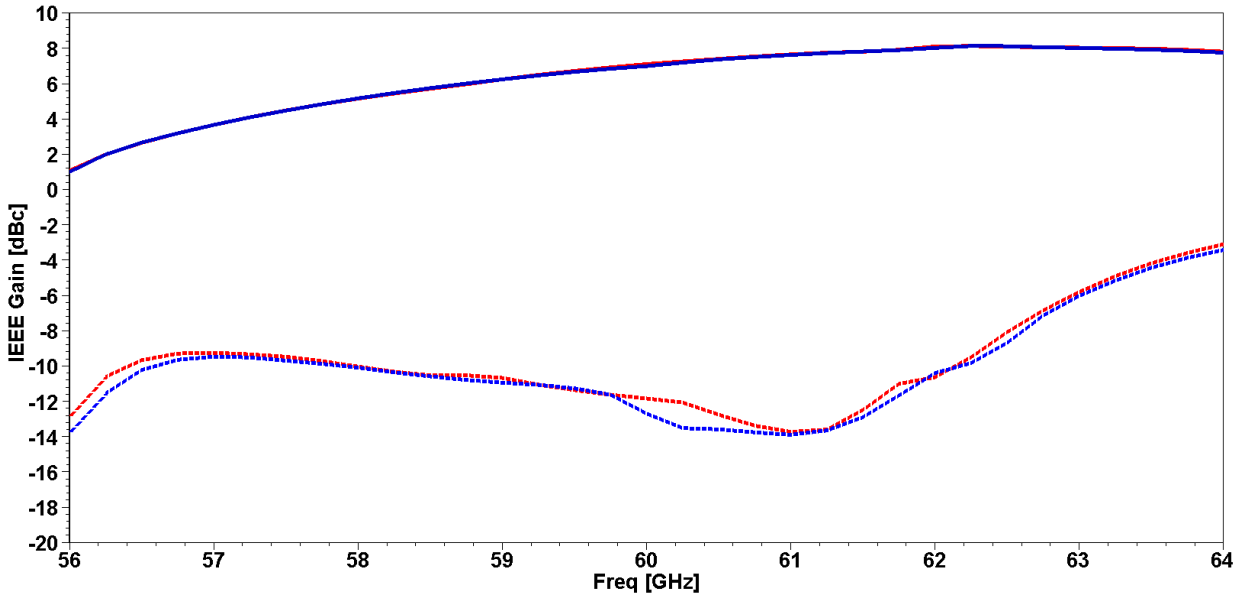

Fig. 3.1.2.6. CP gain for a single element fed with a dielectric-filled waveguide (red) and with SIW (blue). The dotted lines show the cross-polarized gain for the same cases.

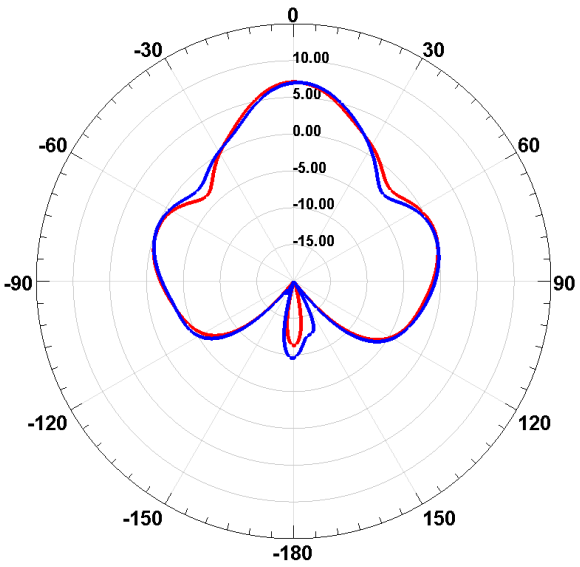

Fig. 3.1.2.7. CP gain pattern for a single element fed with a dielectric-filled waveguide (red) and with SIW (blue) at 60 GHz.

TABLE 3.1.2.2. Single Element Summary Results.

	Dielectric-Filled Waveguide fed	SIW fed
Impedance bandwidth (%)	12.7	12.5
AR Bandwidth (%)	7.4	7.8
Max Gain (dBc)	7.1	7.0
Directivity (dBc)	7.7	7.6
Efficiency (%)	86.5	85.6

3.1.3 Sequentially Rotated Array Antennas

Circularly polarized antennas help to reduce the loss due to polarization mismatch, which is important for off-body communications applications. One method to improve the axial ratio bandwidth with single feed patches is using sequentially rotated arrays. Elements on sequentially rotated arrays can be designed to be linearly polarized or circularly polarized.

Four 2x2 sequentially rotated arrays antenna models were created using LP and CP elements. On both cases, the base design is a square microstrip patch. The patches were designed to operate at a 60 GHz central frequency an air substrate 0.254 mm thick, and using lumped ports for feeding. CP elements consist of square patches with truncated corners and a single feed point; the LP elements have a single feed point. Both phase distributions

of 0°, 90°, 180°, 270°, and 0°, 90°, 0°, 90° were considered for each patch type. Fig. 3.1.3. shows the four array configurations. The dots in the patches represent the feed position in each element.

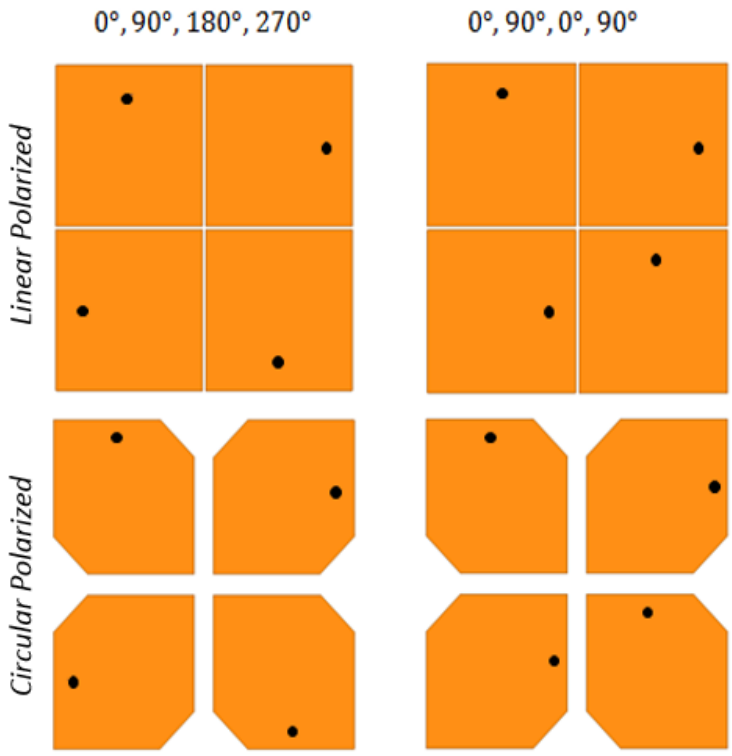

Fig. 3.1.3. Array design for sequentially rotated methods.

3.1.3.1 Linearly and Circularly Polarized Single Elements

The single element patches for CP and LP have a reflection coefficient behavior shown in Fig. 3.1.3.1.1. The red curve is the LP element reflection coefficient, and the blue curve is the reflection coefficient for the CP element. The LP element has an impedance bandwidth of 6.5%, from 58.1 GHz to 62 GHz, and CP element has an impedance bandwidth of 12.8%, from 57.2 GHz to 65 GHz. The axial ratio for the CP element is shown in Fig. 3.1.3.1.2.

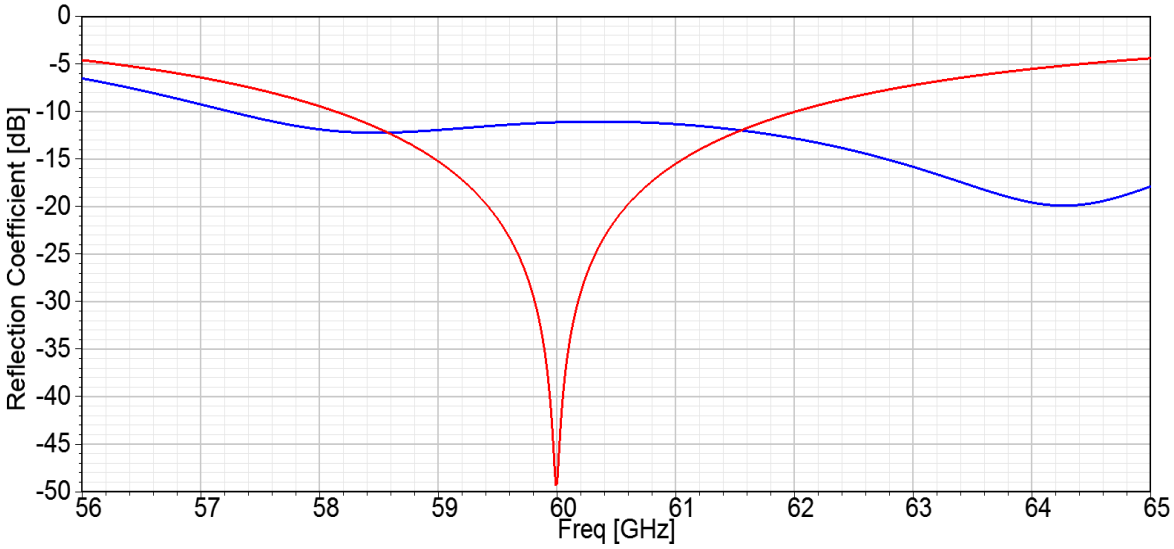

Fig. 3.1.3.1.1. Reflection coefficient for LP element (red) and CP element (blue).

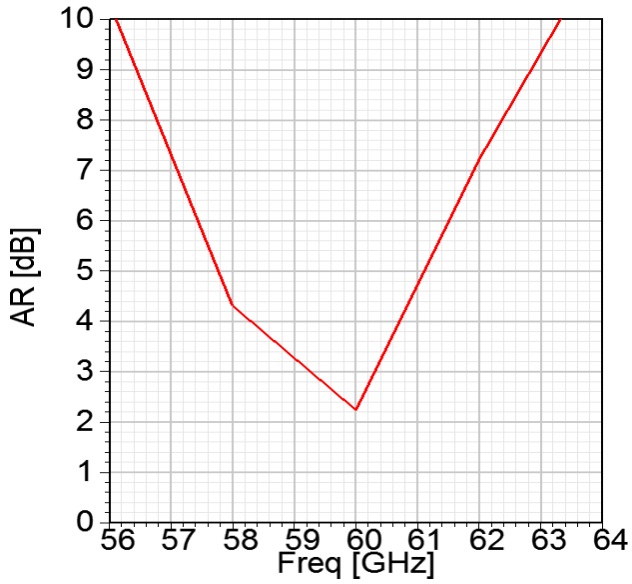

Fig. 3.1.3.1.2. Axial ratio for the CP element.

3.1.3.2 Linearly and Circularly Polarized Arrays

The 2x2 sequentially rotated arrays for CP and LP main differences came from the single element polarization. Fig. 3.1.3.2.1 shows CP gain of the array configurations when the distance between elements is varied. The phase distributions used does not have a significant effect in the array performance. The CP array configurations show a gain of 6 dBc above the LP array configurations. The electric field vectors for both configurations are shown in Fig.

3.1.3.2.2. as the phase progresses. Note that there is no energy in two of the patches when the phase is 45° and 132°. On the other hand, all patches have energy in the CP as the phase progresses, which explain the 6 dB difference in gain between the LP elements and CP elements arrays.

In the four sequentially rotated configurations the axial ratio bandwidth covers the entire band of interest from 55 to 64 GHz. The axial ratio bandwidth is shown in Fig. 3.1.3.2.3. where all the configurations have an AR lower than 1 dB. Comparing all the results from the simulations of the four configurations, is concluded that using a CP single element for the sequentially rotated to array improves the antenna gain as well the axial ratio bandwidth.

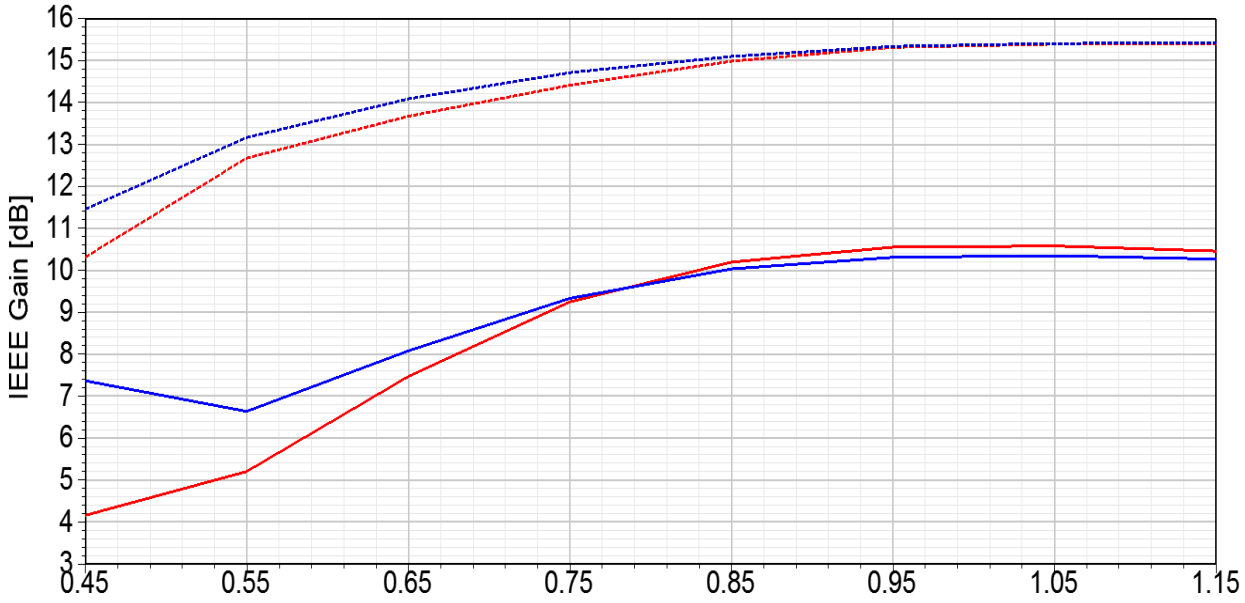

Fig. 3.1.3.2.1. CP gain LP and CP arrays sequentially rotated as function of distance between elements. The CP array 0°, 90°, 180°, 270° (blue dotted), CP array 0°, 90°, 0°, 90° (red dotted), LP array 0°, 90°, 180°, 270° (blue), LP array 0°, 90°, 0°, 90° (red).

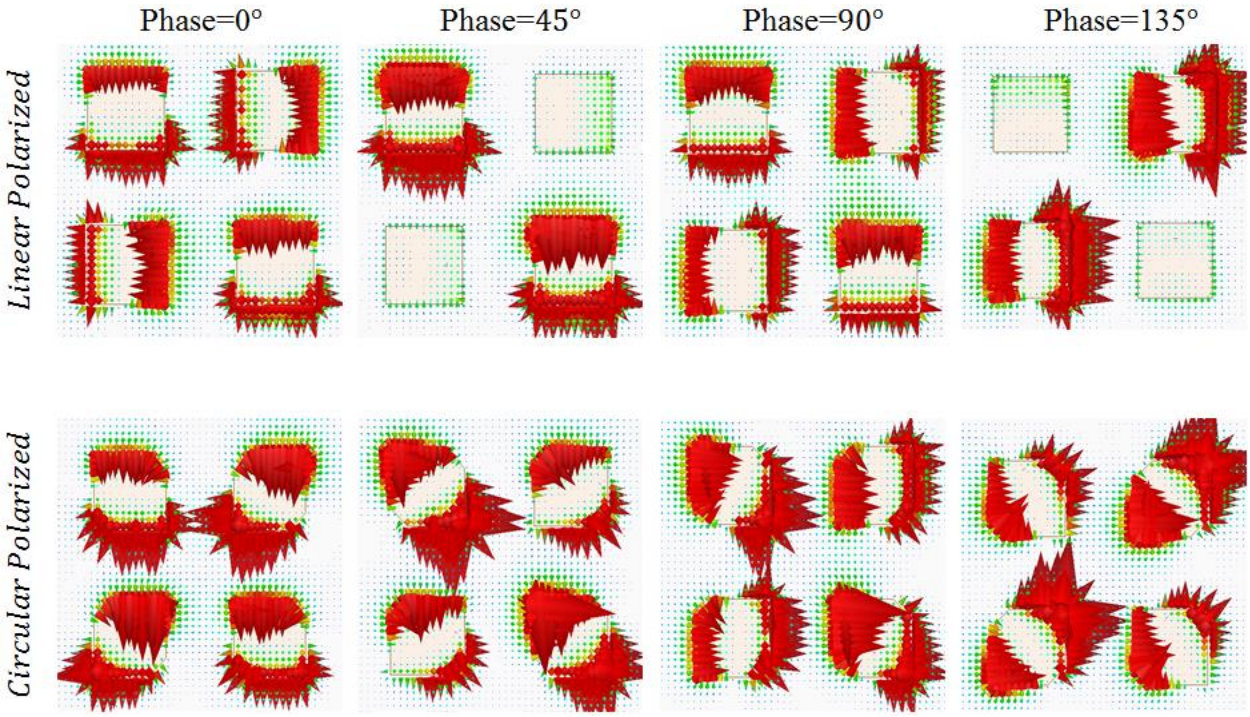

Fig. 3.1.3.2.2. Electric fields vectors for the LP and CP arrays over the patches for different phases.

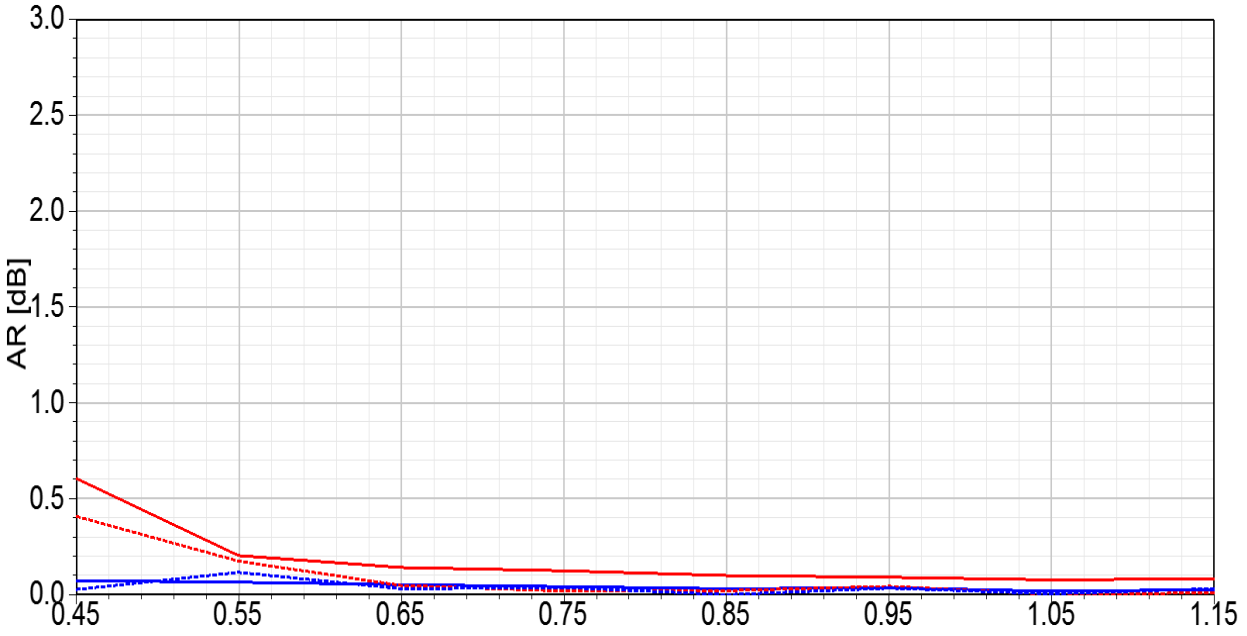

Fig. 3.1.3.2.3. Axial Ratio vs separations between elements in the arrays.

3.1.4 2x2 Array Antenna

Following the element design from the previous section, a 2x2 sequentially rotated array was designed by placing the four elements in vertices of a square. Given that element is left hand circularly polarized (LHCP), the patches were rotated by 90 degrees from each other, moving in a counter-clockwise fashion in the array, as shown in Fig. 3.1.4.1. Furthermore, the elements were fed with a 90 degree phase progression. This section follows the organization of the previous one, and also compare the results from a dielectric-filled waveguide feed (red curves in the figures) and SIW feed (blue curves in the figures).

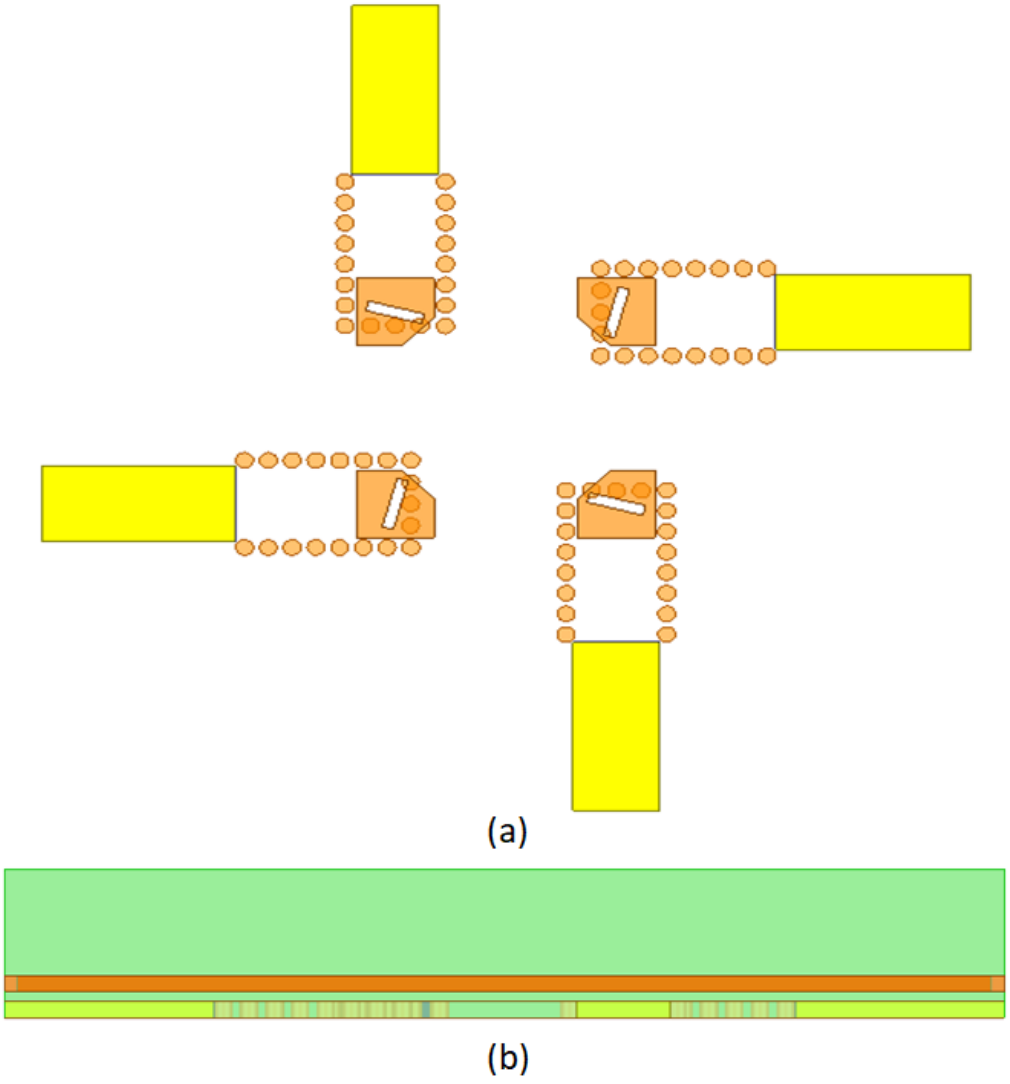

Fig. 3.1.4.1. (a) Top and (b) side view of the 2x2 array using elements describes on Fig. 3.1.2.1.

The element spacing in the array was varied to find the best results in terms of axial ratio, CP gain and bandwidth for the project. Fig. 3.1.4.2. shows the CP gain as the element separation is varied from 0.4λ to 1.10λ. When the separation is lower the gain is lower, but the beam-forming capabilities are greater. On the other hand, the gain increases when the separation is greater. Since the array is not required to greatly steer the beam, the 0.75λ separation was selected. The reflection coefficient and Z parameters for this configuration are shown in Fig.3.1.4.3, and Fig. 3.1.4.4. The 2x2 array reflection coefficient is less than -10 dB from 56 GHz to 62.7 GHz (11.3%). The impedance bandwidth of the single element was 12.5%, and the 2x2 array were reduced to an 11.3%. The results for the axial ratio are shown in Fig. 3.1.4.5, and Fig. 3.1.4.6. The axial ratio bandwidth is greatly improved, because of the sequential rotation method. The axial ratio is lower than 3 dB for the radiation pattern, going from $-16°$ to $16°$ in theta.

The CP gain at 0.75λ separation between elements is shown in Fig. 3.1.4.7, and Fig. 3.1.4.8. The circular gain has been increased about 6 dBc from the single element with a CP gain of 13.6 dBc. The radiation pattern is shown in Fig. 3.1.4.9. Finally, the radiation efficiency of the 2x2 array without considering the long dielectric-filled waveguide or SIW feeds is shown in Fig. 3.1.4.10. Table 3.1.4.1. summarizes the results data.

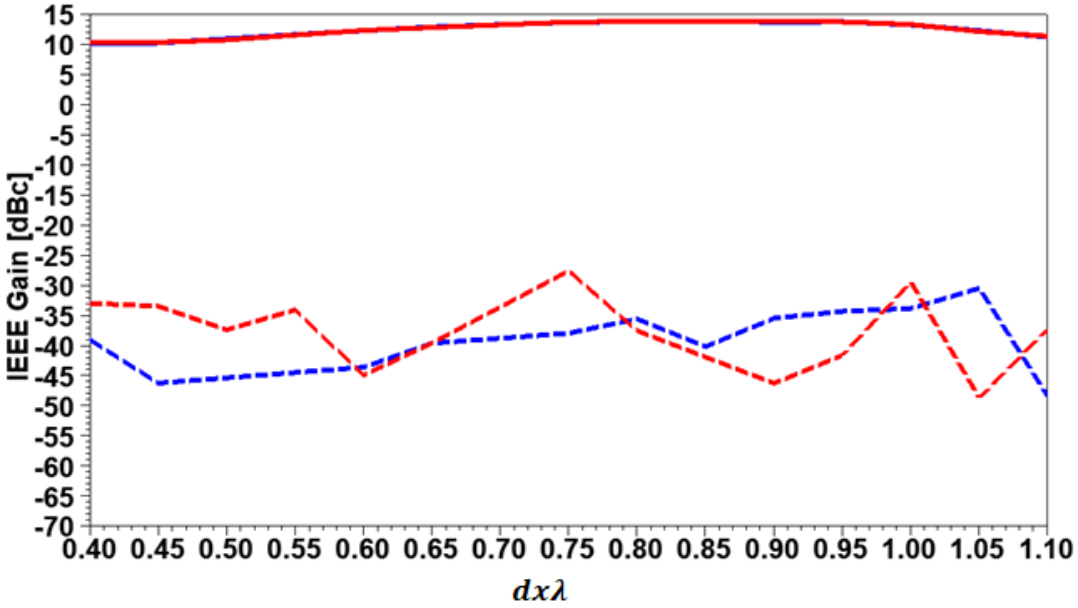

Fig. 3.1.4.2. CP gain variation with element separation for the elements fed with a dielectric-filled waveguide (red) and with SIW (blue) at 60 GHz. The dotted lines show the cross-polarized gain for the same cases.

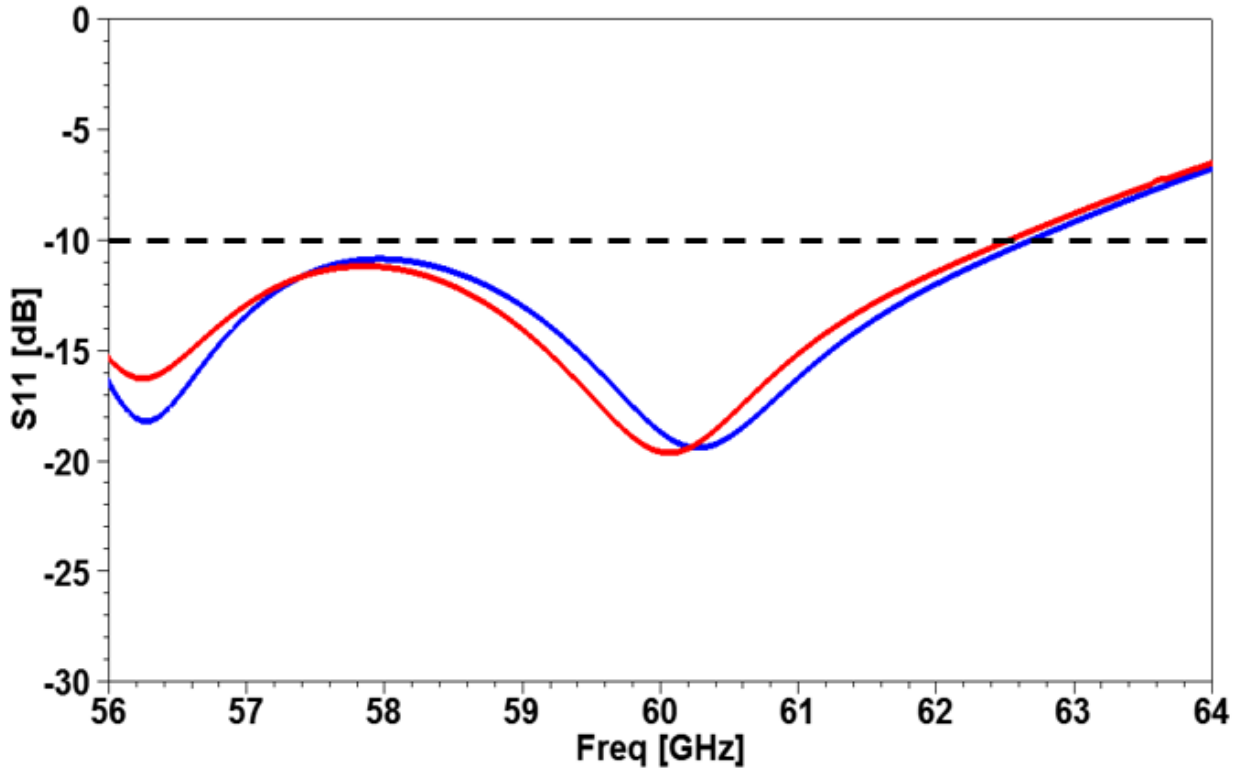

Fig. 3.1.4.3. Reflection coefficient for the 2x2 array for the elements fed with a dielectric-filled waveguide (red) and with SIW (blue).

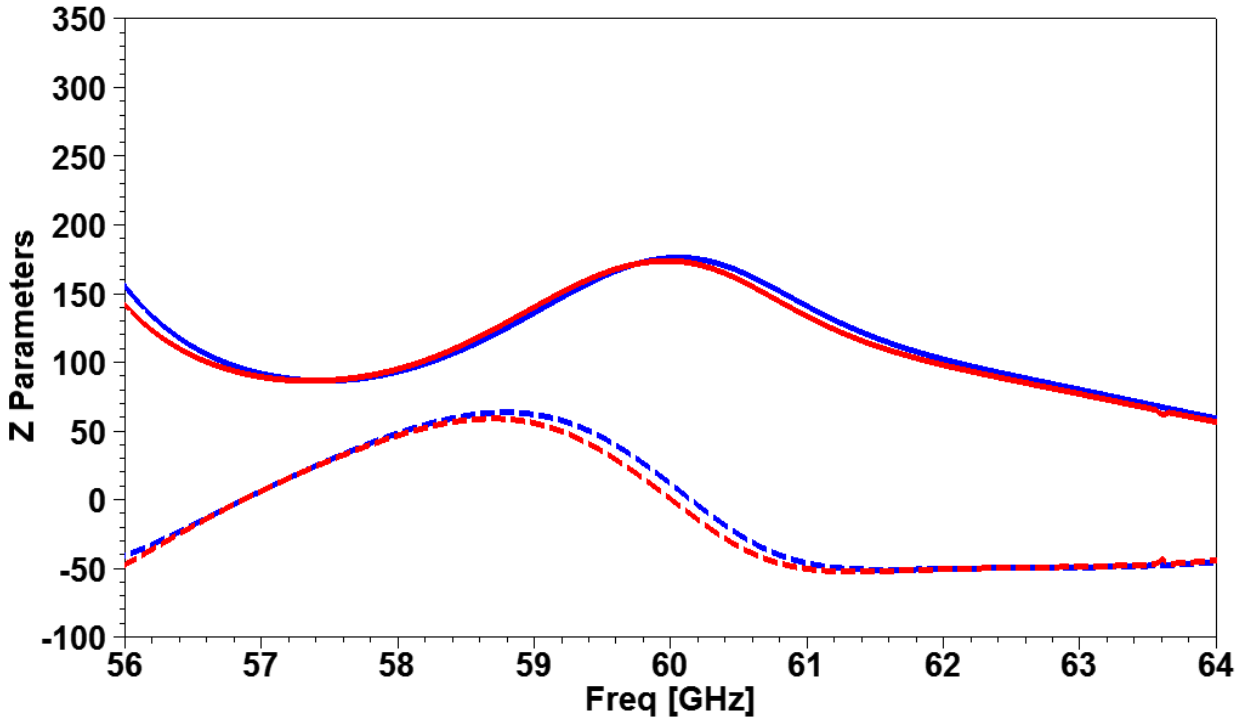

Fig.3.1.4.4. Z11 parameters for the 2x2 array for the elements fed with a dielectric-filled waveguide (red) and with SIW (blue). The solid lines represent the resistance, and the dotted lines show reactance.

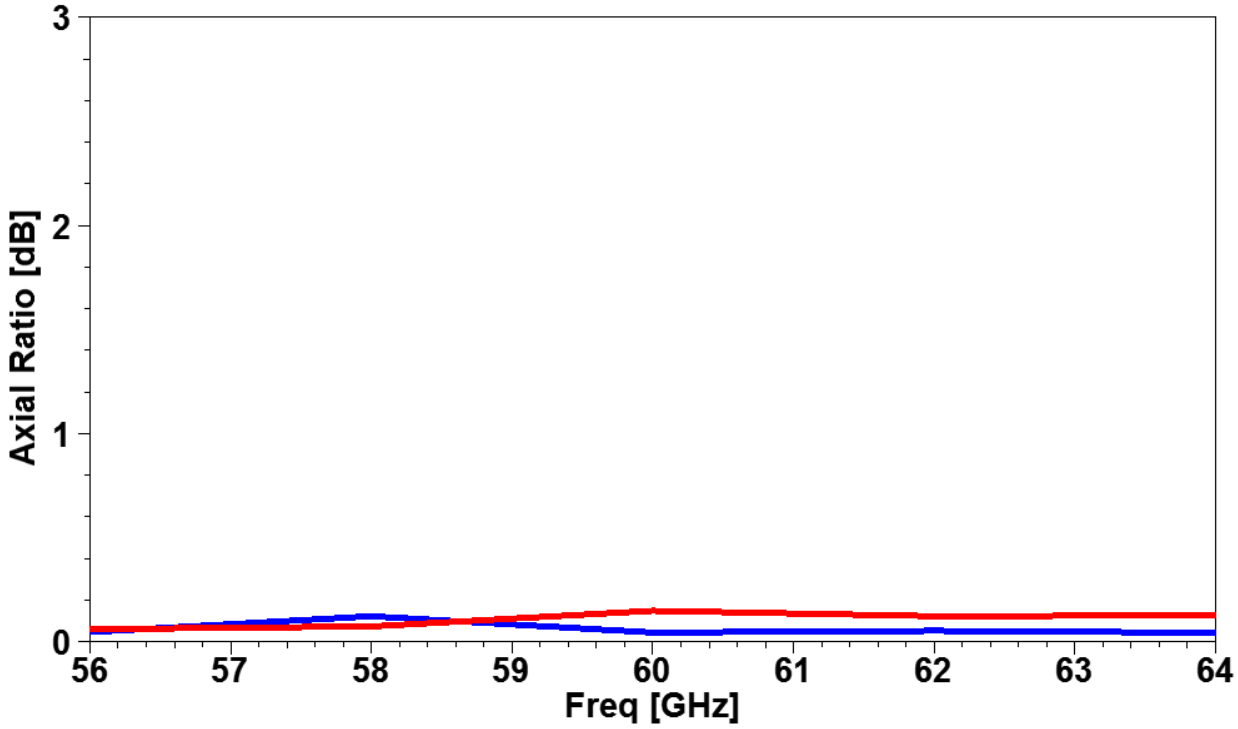

Fig.3.1.4.5. Axial ratio as function of frequency for the 2x2 array for the elements fed with a dielectric-filled waveguide (red) and with SIW (blue).

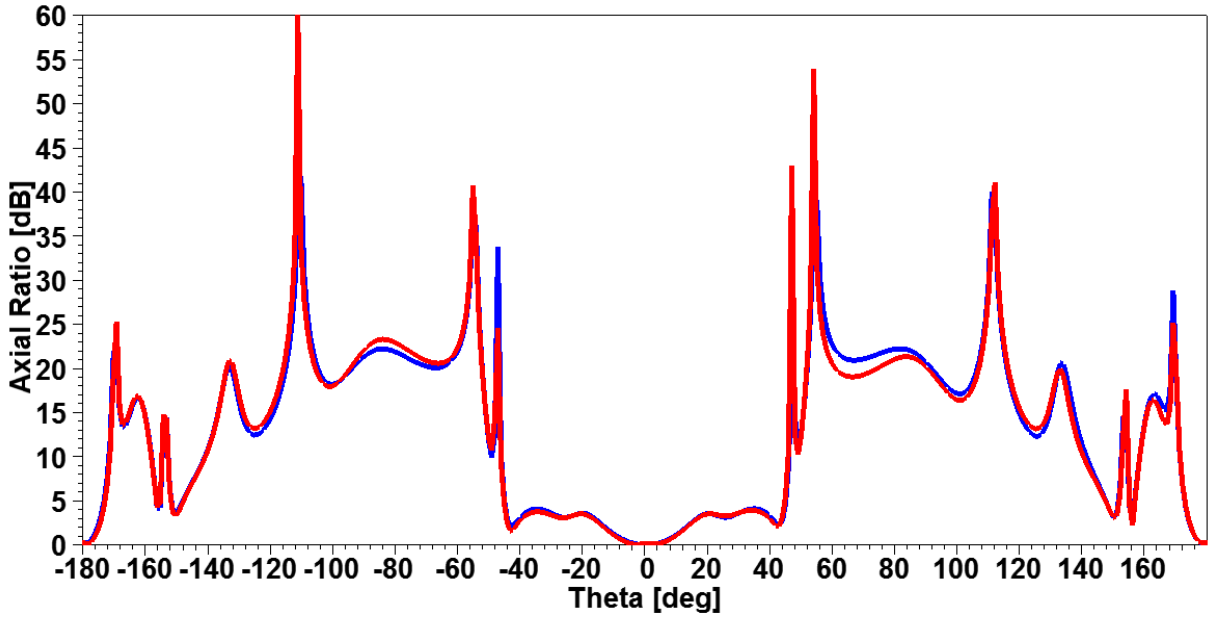

Fig.3.1.4.6. Axial ratio for the 2x2 array as a functions of theta for the elements fed with a dielectric-filled waveguide (red) and with SIW (blue) at 60 GHz.

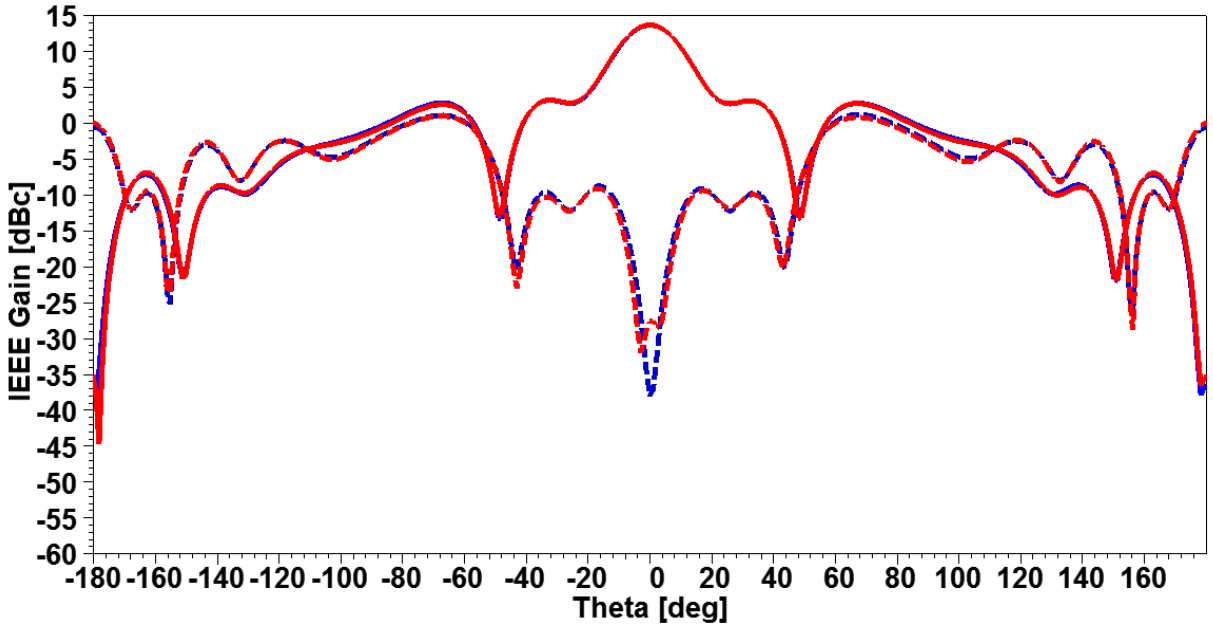

Fig.3.1.4.7. CP gain pattern for the 2x2 array for the elements fed with a dielectric-filled waveguide (red) and with SIW (blue) at 60 GHz. The dotted lines show the cross-polarized gain for the same cases.

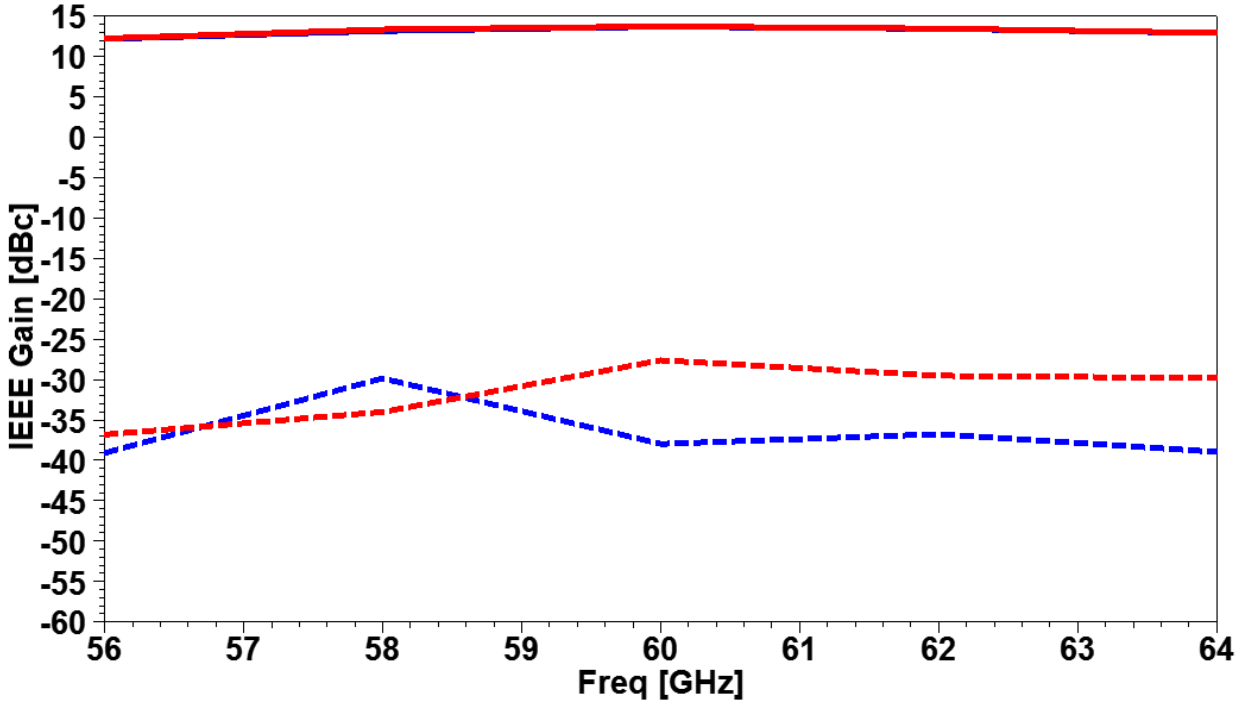

Fig.3.1.4.8. CP gain as a functions of frequency for the 2x2 array antenna for the elements fed with a dielectric-filled waveguide (red) and with SIW (blue). The dotted lines show the cross-polarized gain for the same cases.

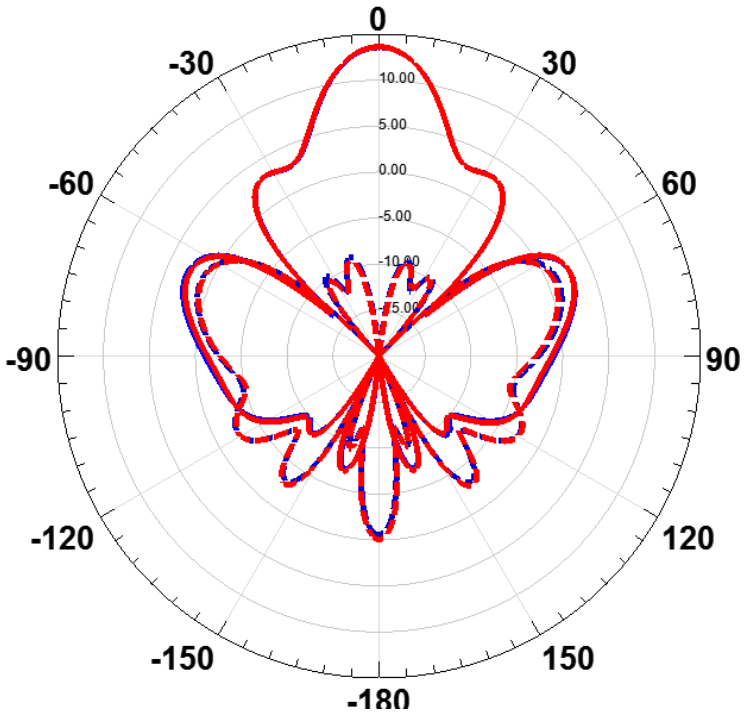

Fig.3.1.4.9. CP gain pattern for the 2x2 array for the elements fed with a dielectric-filled waveguide (red) and with SIW (blue) at 60 GHz. The dotted lines show the cross-polarized gain for the same cases.

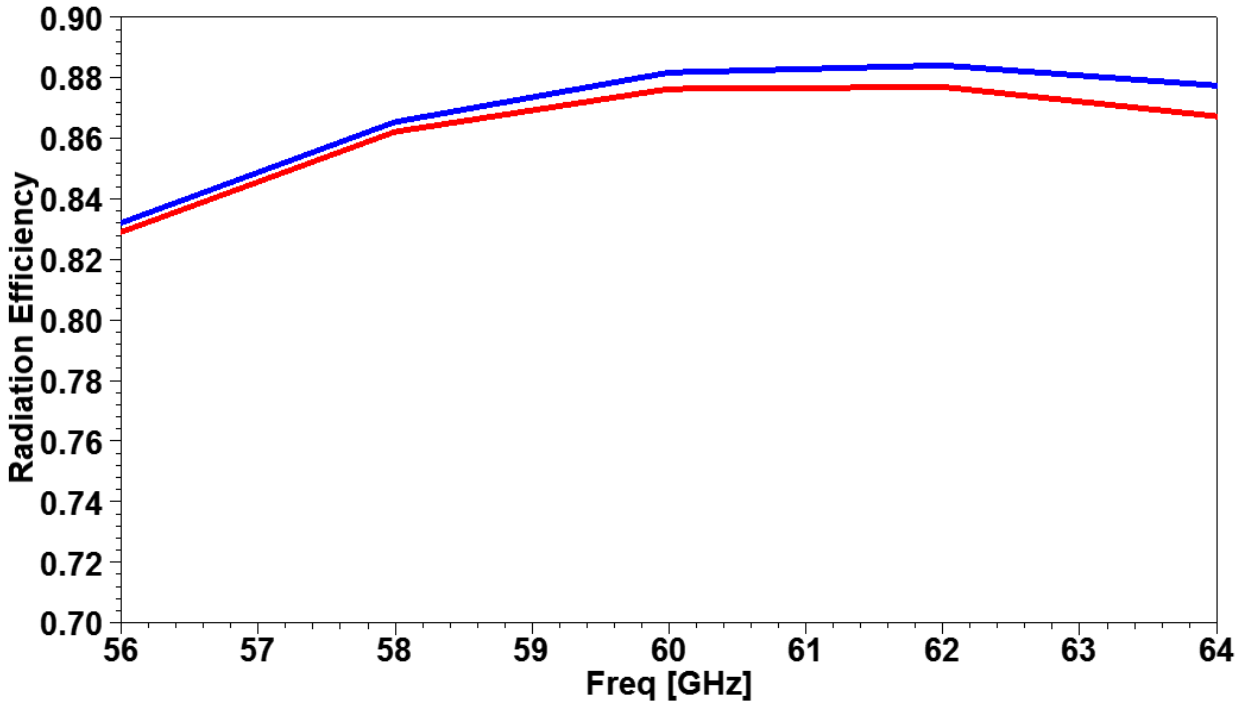

Fig. 3.1.4.10. Radiation efficiency as a functions of frequency for the 2x2 array for the elements fed with a dielectric-filled waveguide (red) and with SIW (blue).

TABLE 3.1.4.1. 2x2 Array Summary Results.

	Dielectric-Filled Waveguide Fed	SIW Fed
S11 (%)	11.0	11.3
AR Bandwidth (%)	13.3	13.3
Z Parameters	173	176+11j
Max Gain (dBc)	13.6	13.6
Cross Polarization (dBc)	-27.6	-38
Radiation Efficiency (%)	87.6	88.1

3.2 Antenna at 60 GHz using FCC Unlicensed Band

3.2.1 Antenna Desired Operation

The proposed antenna is designed to operate in the 57 to 64 GHz band, as specified by the Federal Communication Commission (FCC) 13-112 [14]. The antenna is designed using Ansys High Frequency Structure Simulator (HFSS). The antenna design must have circular polarization with wideband axial ratio, as well as wide impedance bandwidth. The antenna will be fed using SIW fed to reduce backward radiation, since it will be used for BANs application. At the same time, the analysis must consider fabrication tolerances.

3.2.2 Single Element Design

In section 3.1.2 the single element antenna was presented with an operating band that complies with the bandwidth specified in the IEEE 802.11ad standard. The proposed antenna operates from 55.3 GHz to 62.8 GHz and axial ratio from 58.2 GHz to 62.7 GHz. In this case, the antenna already designed was modified to operate in the 57 GHz to 64 GHz FCC unlicensed band. Furthermore, the axial ratio covers most of the band, concentrating in the central frequency.

The Rogers RO 5880 to substrate height of 1.7mm was changed to the Rogers standard substrate height of 1.702mm. The element dimensions were changed to better cover the FCC frequency band. Fig. 3.2.2.1 shows the model for the SIW fed ACMPA with a parasitic patch for the FCC unlicensed band and Table 3.2.2.1 summarizes the different design parameters.

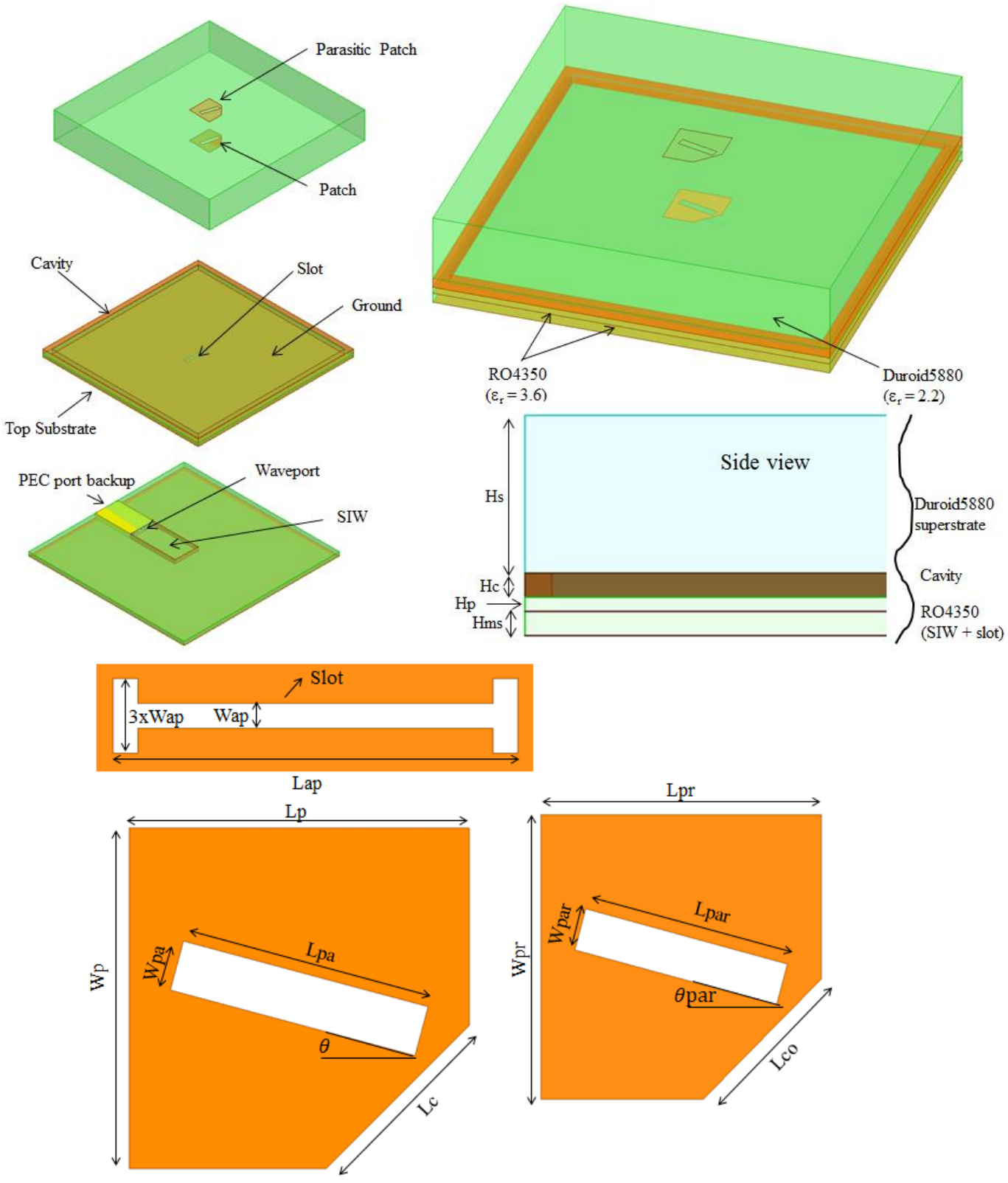

Fig. 3.2.2.1. Antenna design geometry describe by layers. The parameters are summarized in Table 3.2.2.2.

The SIW feed design is the same as the single element from section 3.1.2, but the SIW substrate height was changed from 0.254 mm to 0.422 mm to increase the feed impedance. At 0.422 mm the SIW impedance increases without the need of reducing the width a_{eff} of the SIW to match the antenna impedance. The radiating element and the parasitic have different dimensions to improve the reflection coefficient, as well as the axial ratio bandwidth. The substrate cavity was increased to provide more area for the complete SIW feed and the transition to 1.85 mm coaxial line. The feed transition is discussed in detail in section 3.4.

The single element kept the same restriction of using an H-slot aperture smaller than the width of the radiating element. The dimensions of the H-slot aperture were changed to improve the matching between the antenna and the SIW feed.

TABLE 3.2.2.1. SIW Fed ACMPA Radiation Element Different Parameters.

Parameter	Value	Parameter	Value
H_s	1.702mm	L_{pa}	0.98mm
H_c	0.254mm	θ	15°
H_p	0.168mm	L_c	0.784mm
H_{ms}	0.422mm	W_{pr}	1.34mm
W_{ap}	0.08mm	L_{pr}	1.34mm
L_{ap}	1.25mm	L_{par}	0.997mm
L_p	1.317mm	W_{par}	0.199mm
W_p	1.317mm	L_{co}	0.68mm
W_{pa}	0.196mm	θ_{par}	15°

The reflection coefficient is shown in Fig. 3.2.2.2. Note that -10 dB matching was achieved for the band of interest. The axial ratio bandwidth is shown in Fig. 3.2.2.3. Note that the AR bandwidth covers from 58.1 GHz to 63.7 GHz. Fig. 3.2.2.4. shows the AR as a function of theta at 60 GHz, to verify the feasibility of using this element for beam-scanning applications. The AR is below 3 dB from $-7°$ to 8°. The CP gain at 60 GHz has 6.5 dB

sidelobes at $-26°$ and $27°$, as shown in Fig. 3.3.2.5. Fig. 3.2.2.6 shows the CP gain as a function of frequency. Note that the gain increases from 5.39 dB at 57 GHz to 8.09 dB at 64 GHz. The CP gain at central frequency of 60 GHz is of 8.5 dBc. The gain pattern for the radiating element is shown in Fig. 3.2.2.7. The results for the single radiating elements are summarized in Table 3.2.2.2.

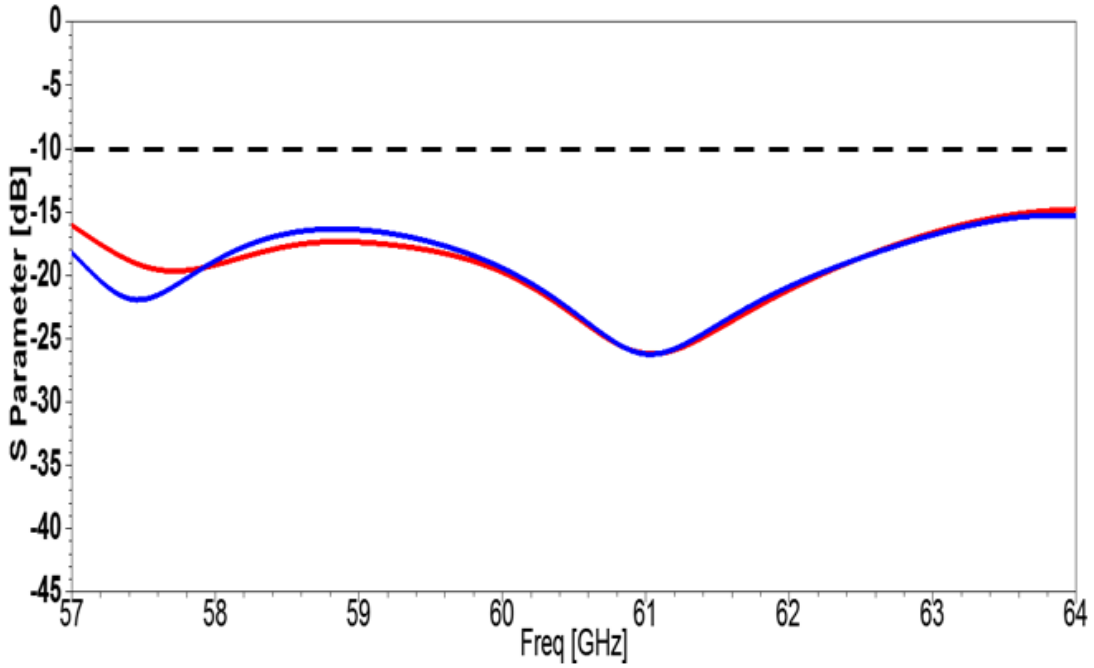

Fig. 3.2.2.2. Reflection coefficient for a single element fed with a dielectric-filled waveguide (red) and with SIW (blue).

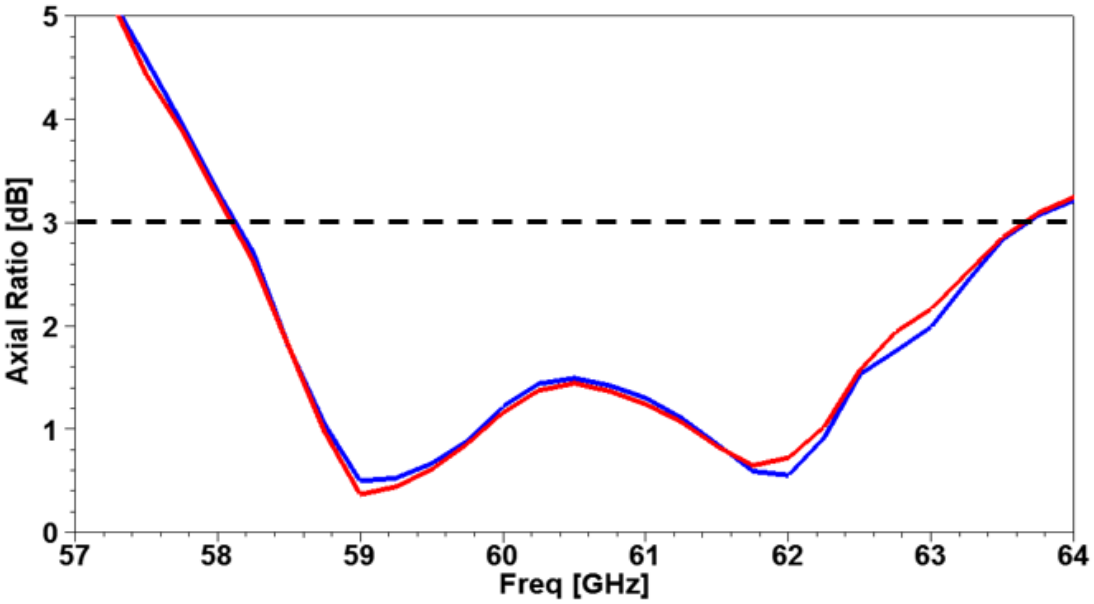

Fig. 3.2.2.3. Axial ratio bandwidth for a single element fed with a dielectric-filled waveguide (red) and with SIW (blue).

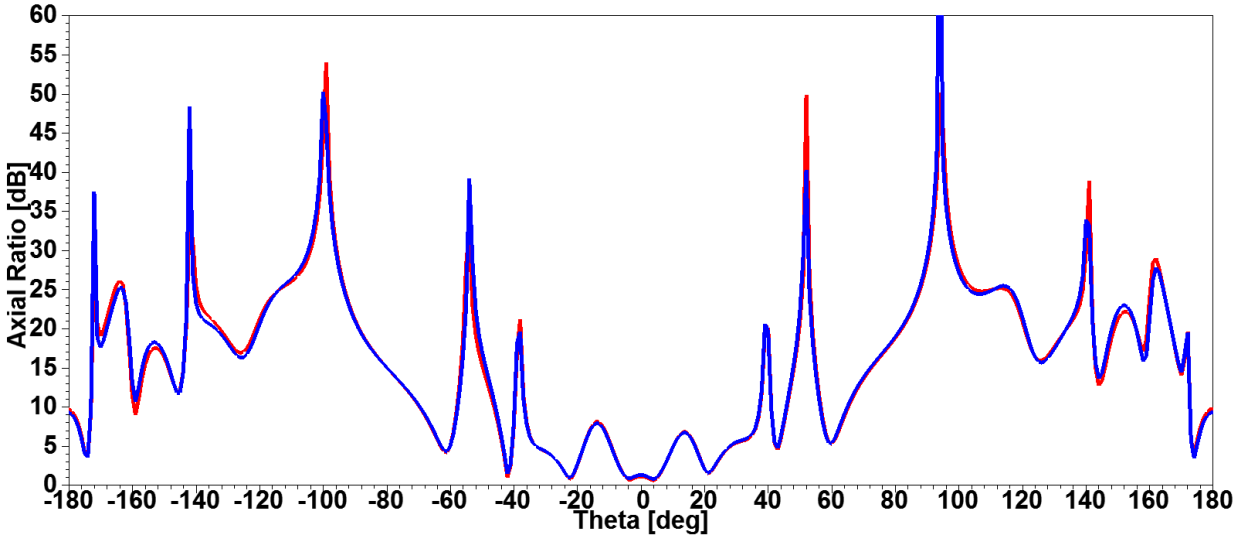

Fig. 3.2.2.4. Axial ratio as a function of theta at 60 GHz for a single element fed with a dielectric-filled waveguide (red) and with SIW (blue).

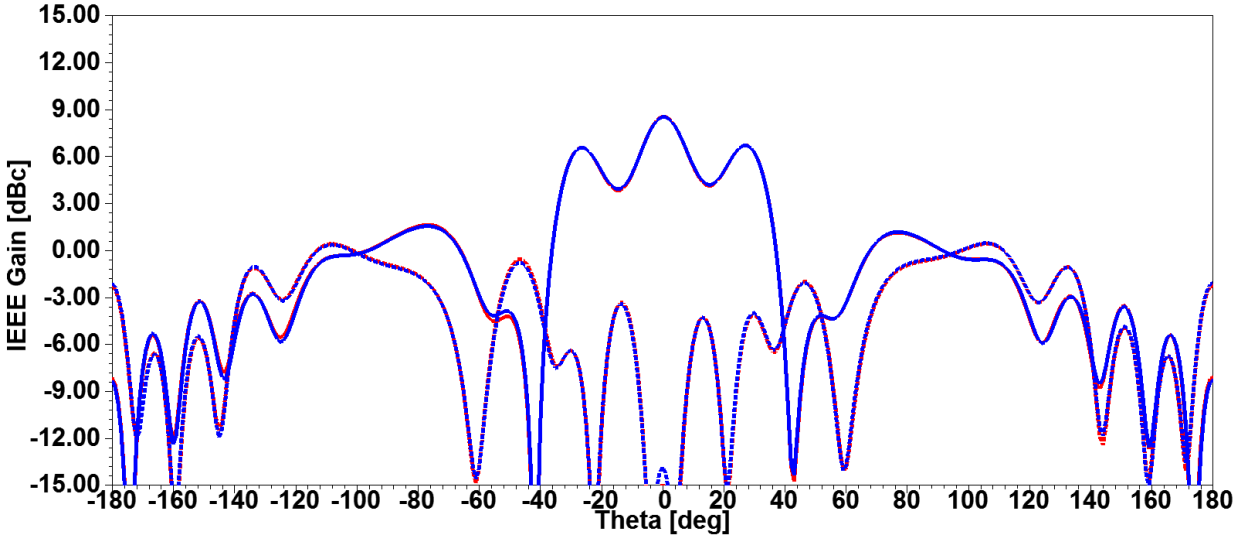

Fig. 3.2.2.5. CP gain pattern for a single element at 60 GHz fed with a dielectric-filled waveguide (red) and with SIW (blue). The dotted lines show the cross-polarized gain for the same cases.

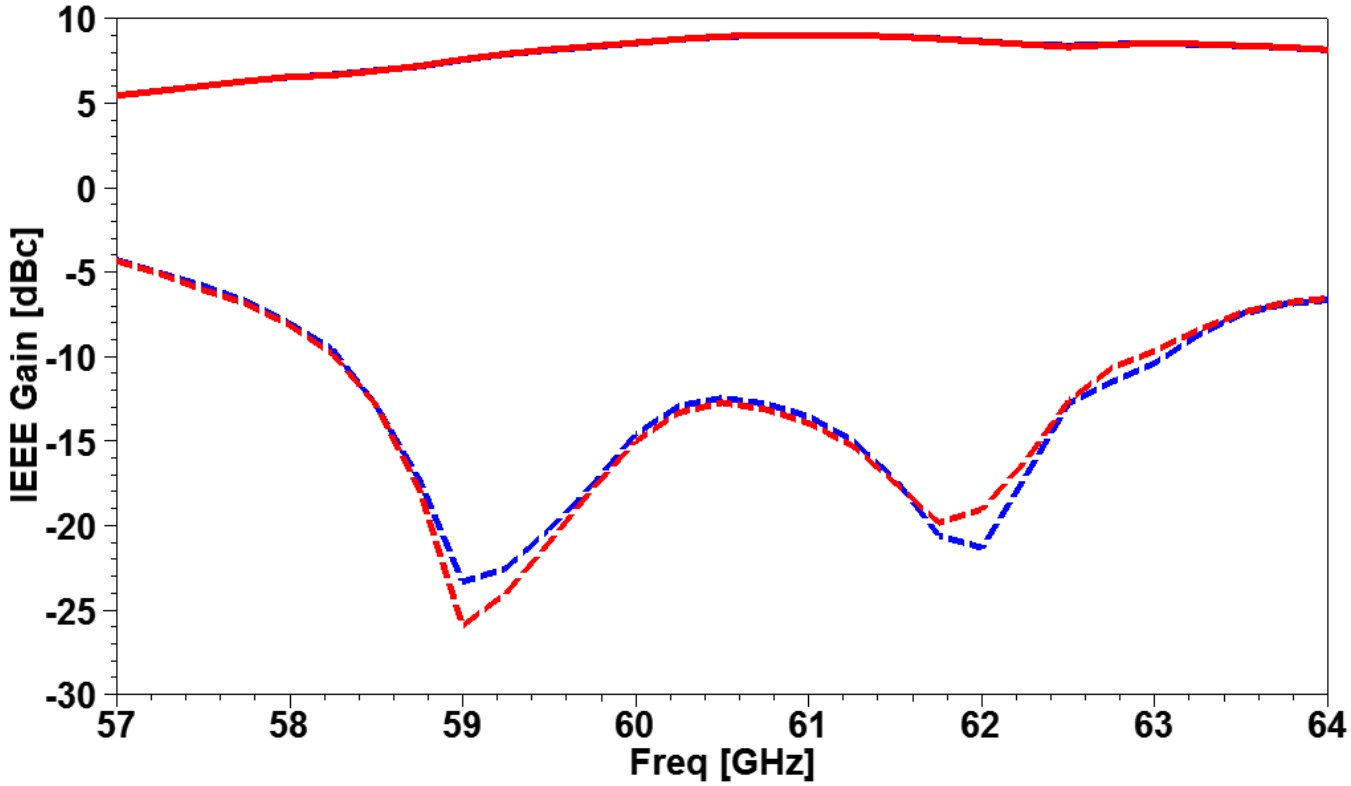

Fig. 3.2.2.6. CP gain for a single element fed with a dielectric-filled waveguide (red) and with SIW (blue). The dotted lines show the cross-polarized gain for the same cases.

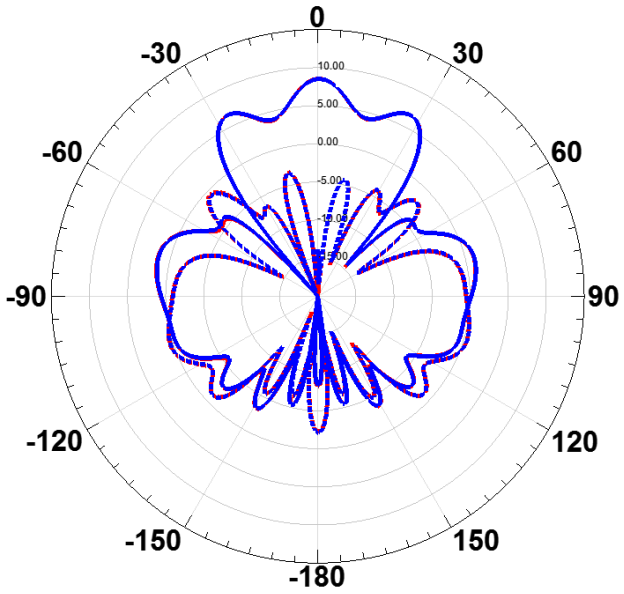

Fig. 3.2.2.7. CP gain pattern for a single element fed with a dielectric-filled waveguide (red) and with SIW (blue) at 60 GHz.

TABLE 3.2.2.2. Single Element Summary Results.

	Dielectric-Filled Waveguide fed	SIW fed
Impedance bandwidth (%)	11.6	11.6
AR Bandwidth (%)	9.2	9.2
Max Gain (dBc)	8.5	8.5
Directivity (dBc)	9.2	9.2
Efficiency (%)	86.2	85.8

3.2.3 2x2 Array Antenna

Following the design from the previous section, a 2x2 array was designed using the array placement discussed in section 3.1.4. Given that the element is left hand circular polarized (LHCP), the patches were rotated 90 degrees as shown in Fig. 3.2.3.1. Furthermore, the elements were fed with a 90 degree phase progression. This section follows the organization of the previous one, and also compares the results from a dielectric-filled waveguide (red curves in the figures) and SIW (blue curves in the figures).

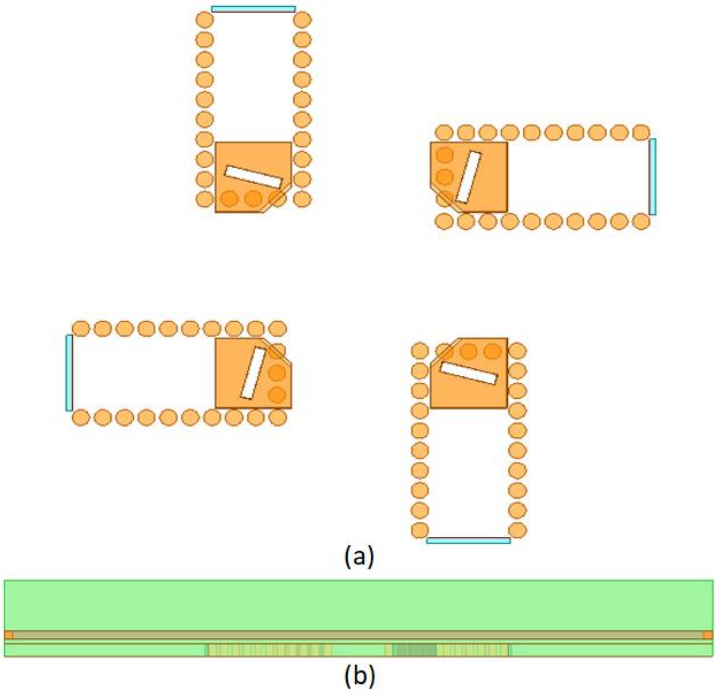

Fig. 3.2.3.1. (a) Top and (b) side view for the 2x2 array with dielectric-filled waveguide and SIW fed. The design was develop from the previous design on fig. 3.2.2.1.

The element spacing in the array was varied to find the best results in terms of axial ratio, CP gain and bandwidth for the project. Fig. 3.2.3.2. shows the CP as the element separation is varied from 0.4λ to 1.10λ. Since the array is not required to greatly steer the beam, the 0.75λ separation was selected. The reflection coefficient and Z parameters for this configuration are shown in Fig. 3.2.3.3, and Fig. 3.2.3.4. The impedance bandwidth keep the same bandwidth of the single element. The axial ratio bandwidth greatly improved, because of the sequentially rotation method. The results for the axial ratio are shown in Fig. 3.2.3.5, and Fig. 3.2.3.6. Note that the AR is less than 3 dB from $-29°$ to $29°$.

The CP gain at 0.75λ separation between elements is shown in Fig. 3.2.3.7, and Fig. 3.2.3.8. The CP gain at the central frequency of 60 is of 12.7 dBc. The CP radiation pattern is shown in Fig. 3.2.3.9. Finally, the radiation efficiency of the 2x2 array without considering long dielectric-filled waveguide or SIW feeds is shown in Fig. 3.2.3.10. Table 3.2.3.1. summarizes the results data.

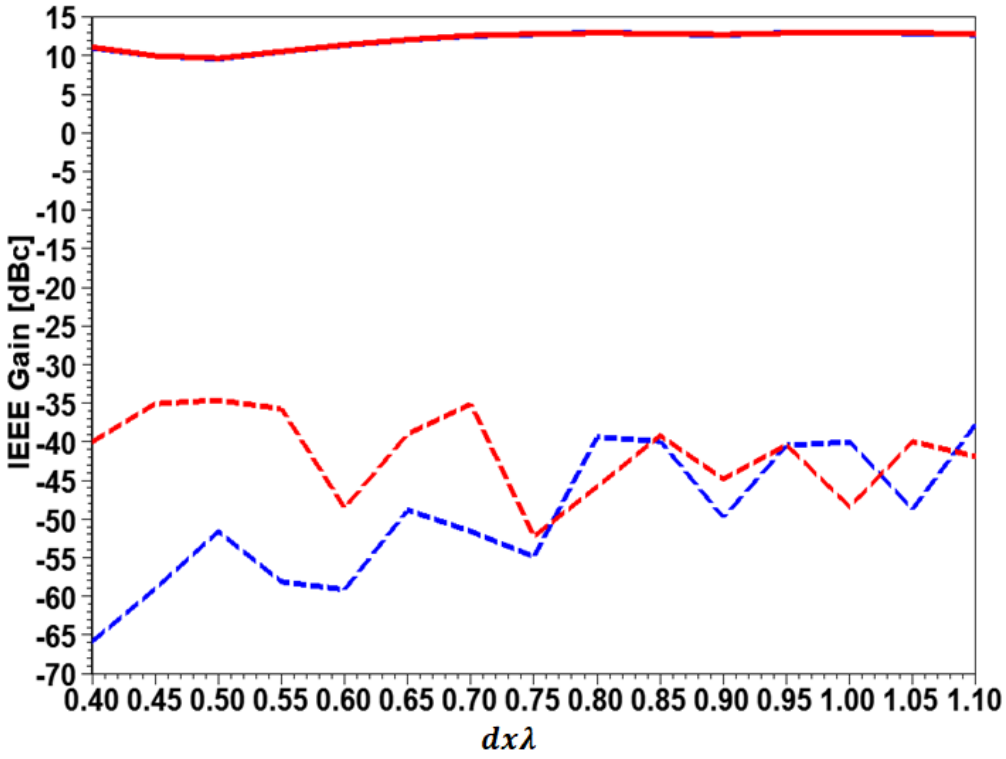

Fig. 3.2.3.2. CP gain variation with element separation for the elements fed with a dielectric-filled waveguide (red) and with SIW (blue) at 60 GHz. The dotted lines show the cross-polarized gain for the same cases.

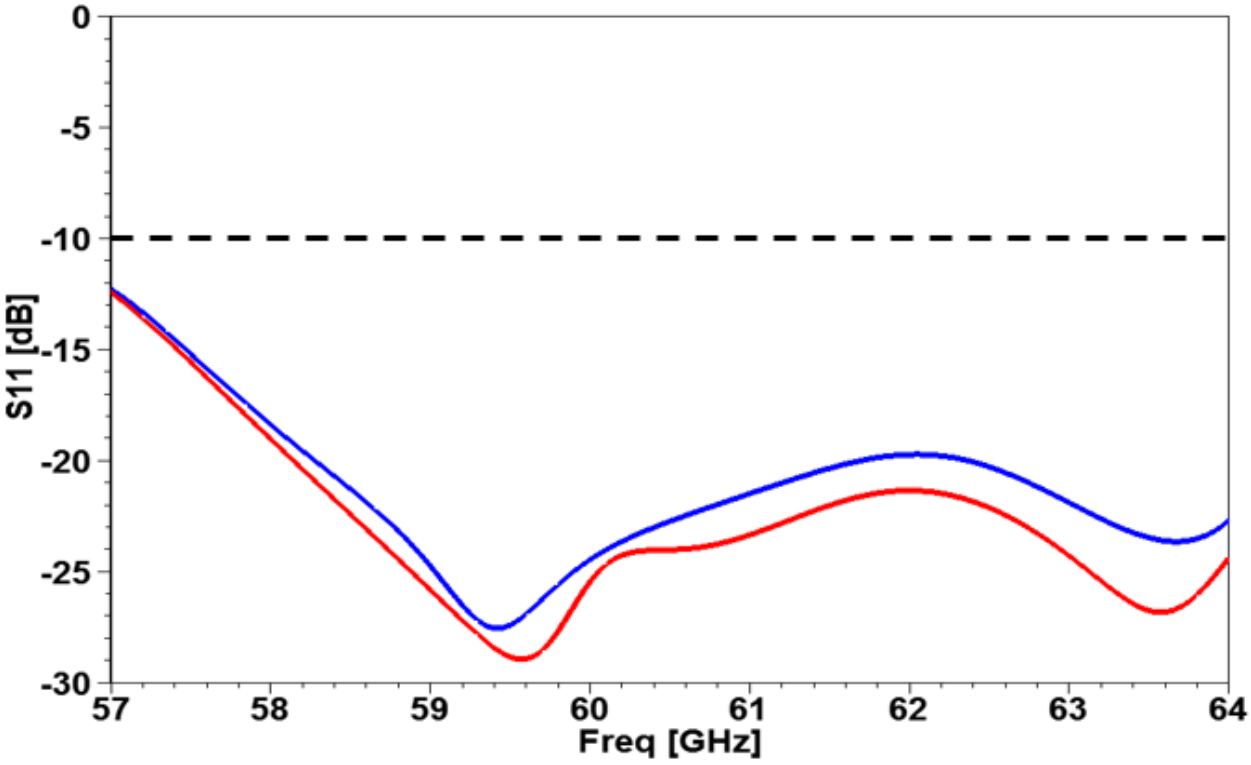

Fig. 3.2.3.3. Reflection coefficient for the 2x2 array for the elements fed with a dielectric-filled waveguide (red) and with SIW (blue).

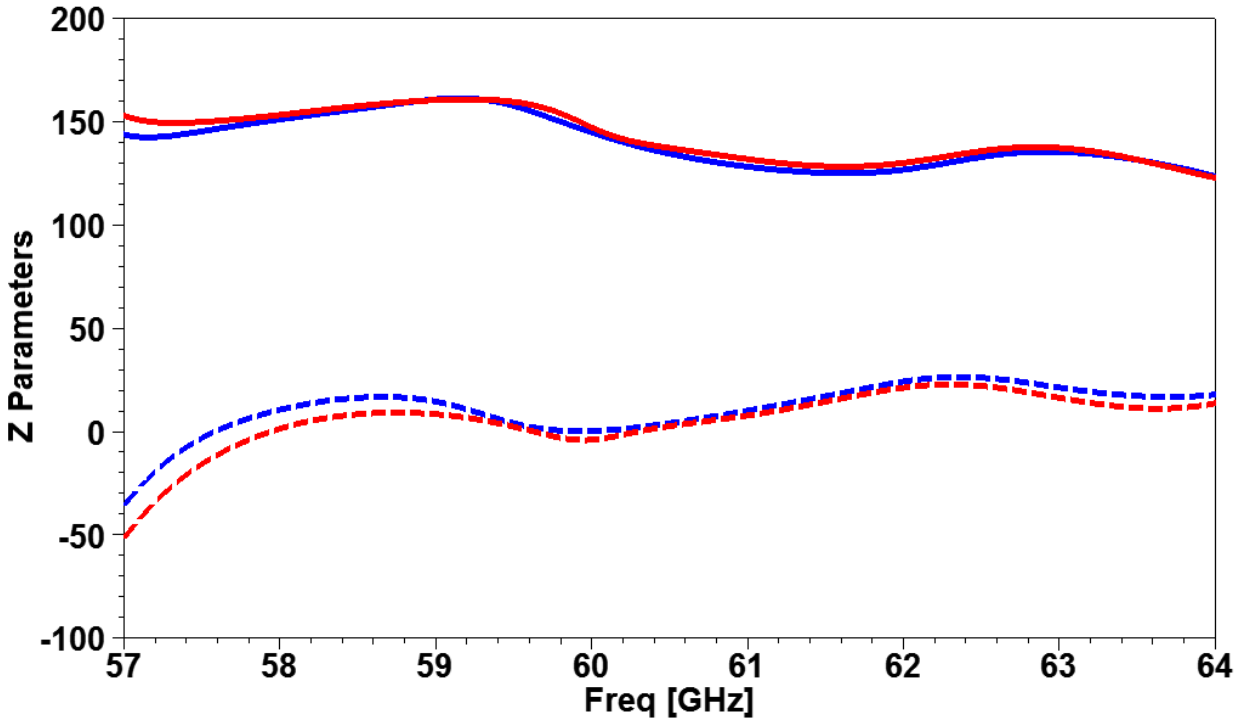

Fig. 3.2.3.4. Z11 parameters for the 2x2 array for the elements fed with a dielectric-filled waveguide (red) and with SIW (blue). The solid lines represent the resistance, and the dotted lines show reactance.

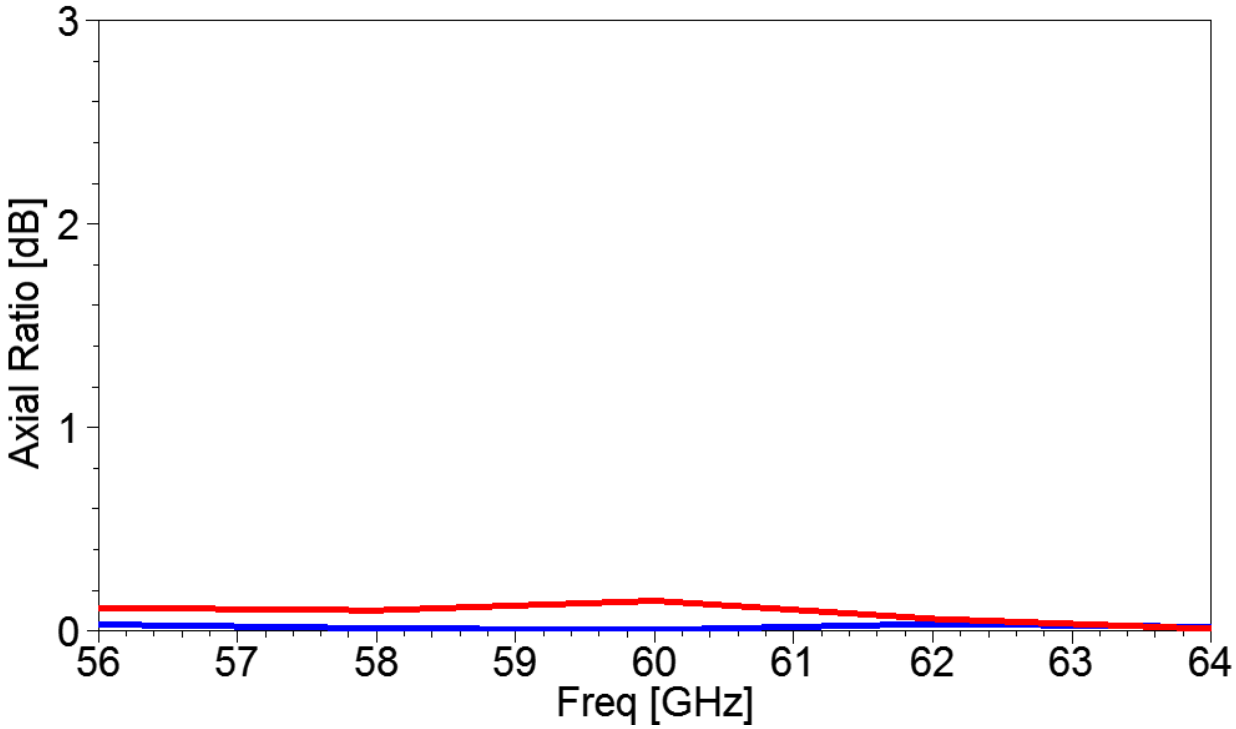

Fig. 3.2.3.5. Axial ratio as a function of frequency for the 2x2 array for the elements fed with a dielectric-filled waveguide (red) and with SIW (blue).

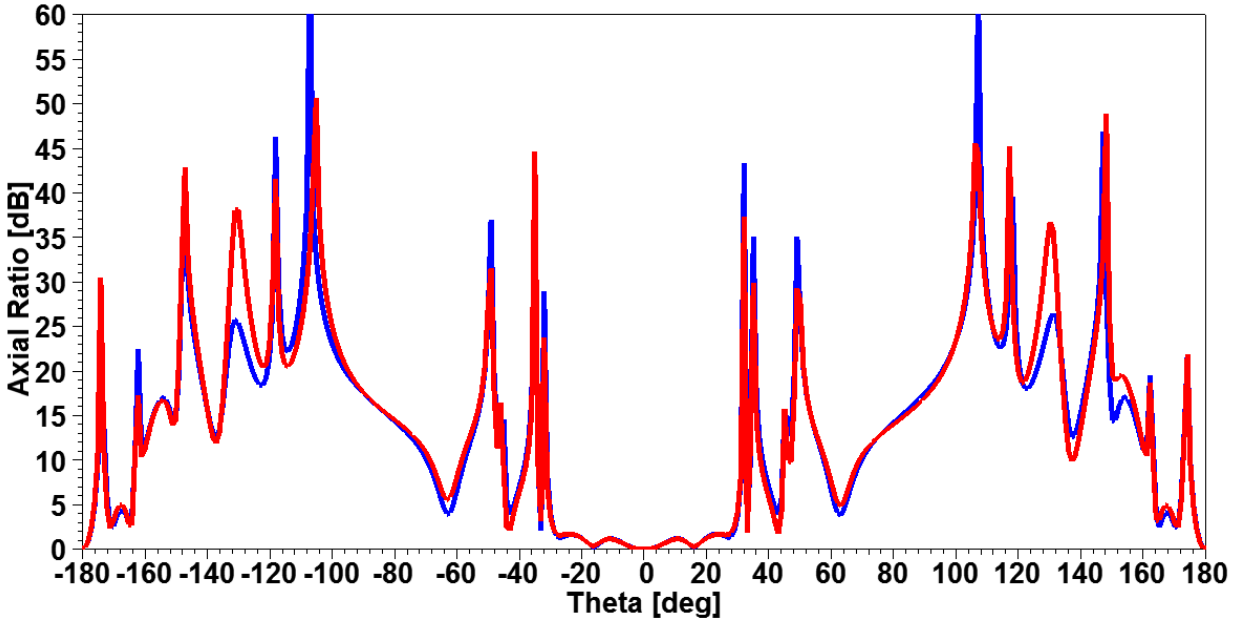

Fig. 3.2.3.6. Axial ratio for the 2x2 array as a function of theta for the elements fed with a dielectric-filled waveguide (red) and with SIW (blue) at 60 GHz.

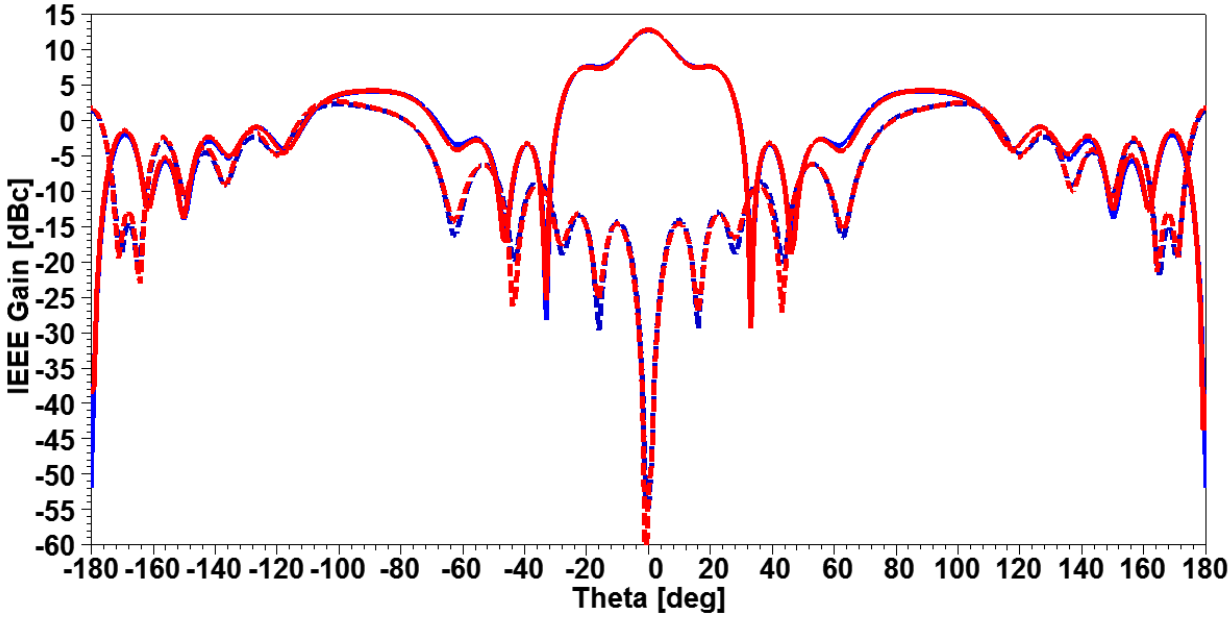

Fig. 3.2.3.7. CP gain pattern for the 2x2 array for the elements fed with a dielectric-filled waveguide (red) and with SIW (blue) at 60 GHz. The dotted lines show the cross-polarized gain for the same cases.

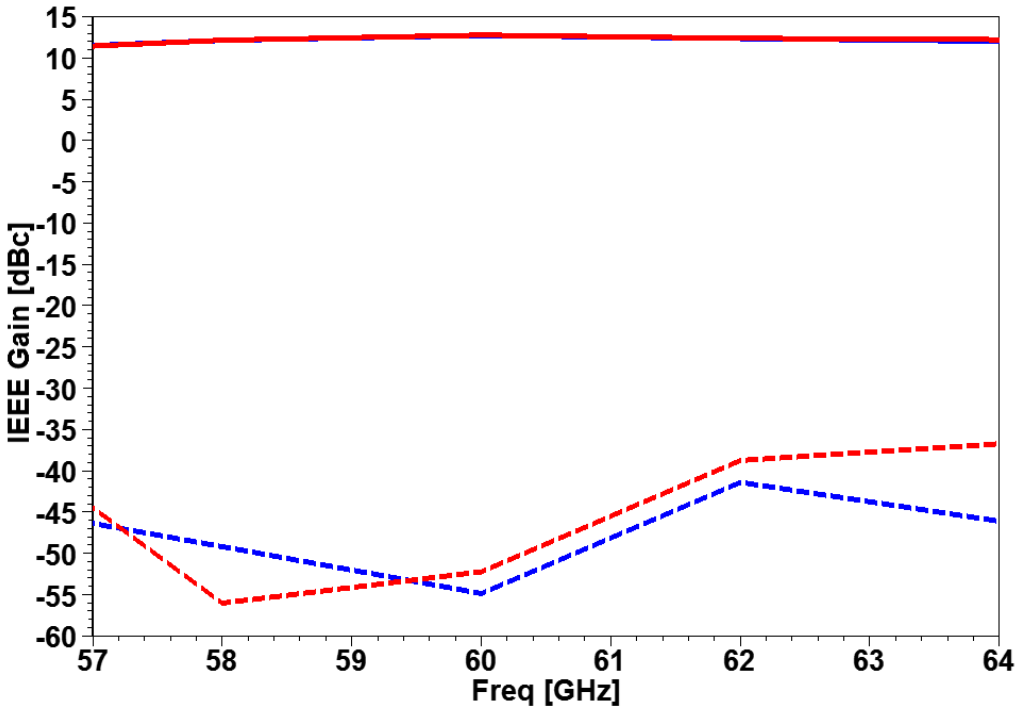

Fig. 3.2.3.8. CP gain as a function of frequency for the 2x2 array antenna for the elements fed with a dielectric-filled waveguide (red) and with SIW (blue). The dotted lines show the cross-polarized gain for the same cases.

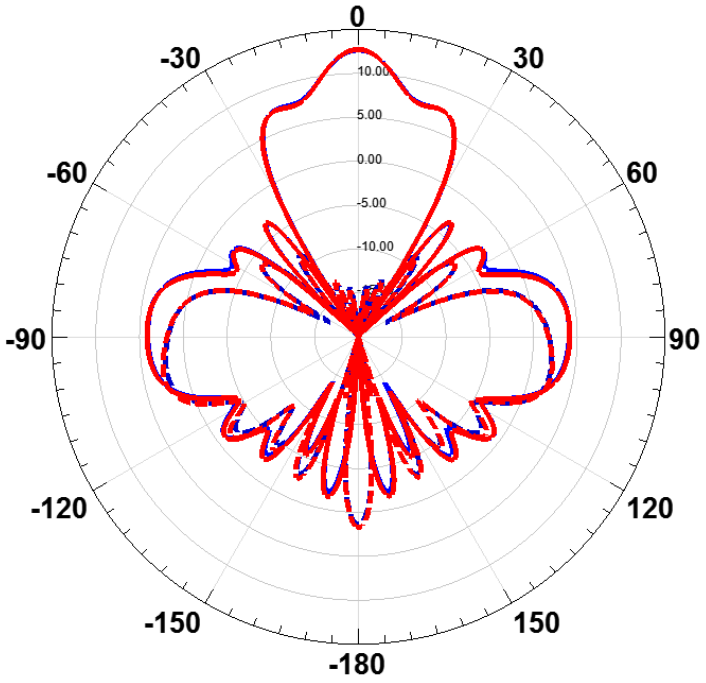

Fig. 3.2.3.9. CP gain pattern for the 2x2 array for the elements fed with a dielectric-filled waveguide (red) and with SIW (blue) at 60 GHz. The dotted lines show the cross-polarized gain for the same cases.

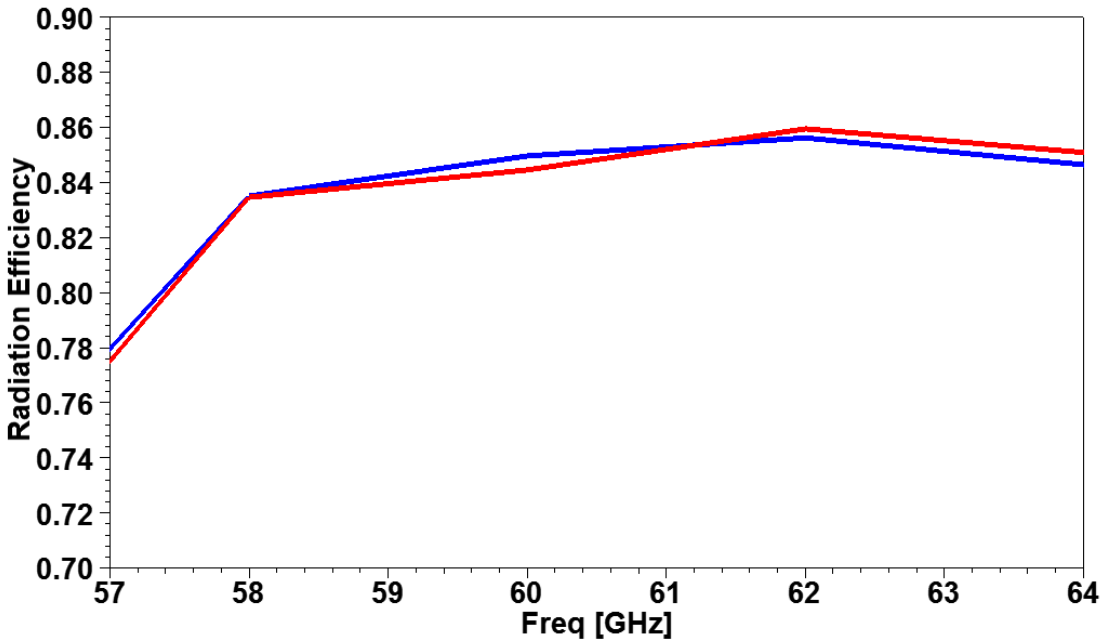

Fig. 3.2.3.10. Radiation efficiency as a function of frequency for the 2x2 array for the elements fed with a dielectric-filled waveguide (red) and with SIW (blue).

TABLE 3.2.3.1. 2x2 Array Summary Results.

	Dielectric-Filled Waveguide Fed	SIW Fed
S11 (%)	11.6	11.6
AR Bandwidth (%)	11.6	11.6
Z Parameters	147-4j	145
Max Gain (dBc)	12.7	12.7
Radiation Efficiency (%)	84.4	84.9

3.3 Feed Line Transition

3.3.1 Single Element Feed Line Transition

To feed the single element presented in sections 3.1.2 and section 3.2.2, a feed line using taper was designed. The circularly polarized single element patches designed have high input impedance around 200 Ω to 220 Ω. Using the feeding aperture helps to reduce the antenna impedance, but it is still necessary to reduce it much more to implement coaxial feed. With this in mind, the feed line transition was design to reduce the antennas impedance to be able to integrate to a coaxial transition line.

Substrate integrated waveguide, as well as the dielectric-filled waveguide, has the same behavior as a hollow waveguide. The height and width of the waveguide determine its characteristic impedance. When the SIW width is varied a range of characteristic impedance is created. This range can be move only if the height of the SIW is changed. If the height of the SIW is increased, the range of the characteristic impedances achievable as the SIW width varied, is increased. The design used to reduce the impedance from the antenna to the coaxial transition is shown in Fig. 3.3.1.1.

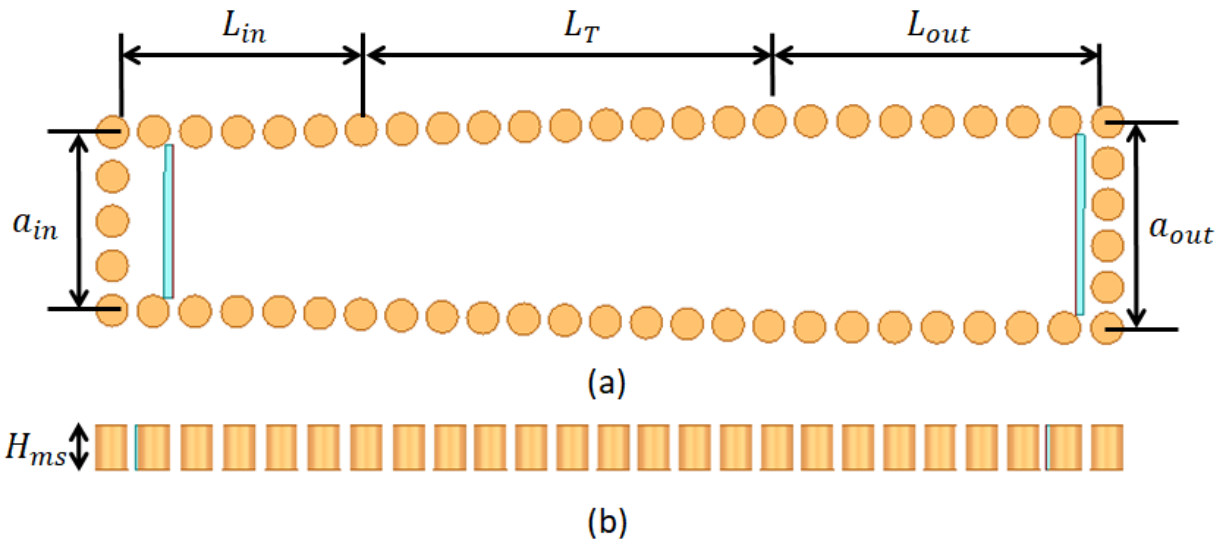

Fig. 3.3.1.1. Feed transition impedance from 165 to 90Ω using taper. (a) Top view model for the design SIW. (b) Side view model.

TABLE 3.3.1.1. Feed Transition Parameters.

Parameter	Value
a_{in}	1.68mm
a_{out}	1.94mm
L_{in}	1.46mm
L_T	5mm
L_{out}	1.76mm
H_{ms}	0.422mm

To reduce the impedance from 165 Ω to 95 Ω a taper was designed, with two straight SIW sections in both ports. The a_{in} section has a characteristic impedance of 162 Ω, while a_{out} has a characteristic impedance of 95 Ω. While both sides of the design are fixed in width and length, the taper was varied in length to reduce reflections. The design was done for both a dielectric-filled waveguide and SIW. Fig. 3.3.1.2 shows the reflection coefficient, and note that it is less than -15 dB in the band of interest. Figs. 3.3.1.3 and 3.3.1.4, show the impedance for both ports against frequency. The impedance of the antenna at the SIW level is about 170 Ω, and it was reduce to 95 Ω using the taper. The wave-ports

were placed under the H-slot aperture couple position. In addition, the wave-ports impedances were set the impedance of the load to be placed at the ends.

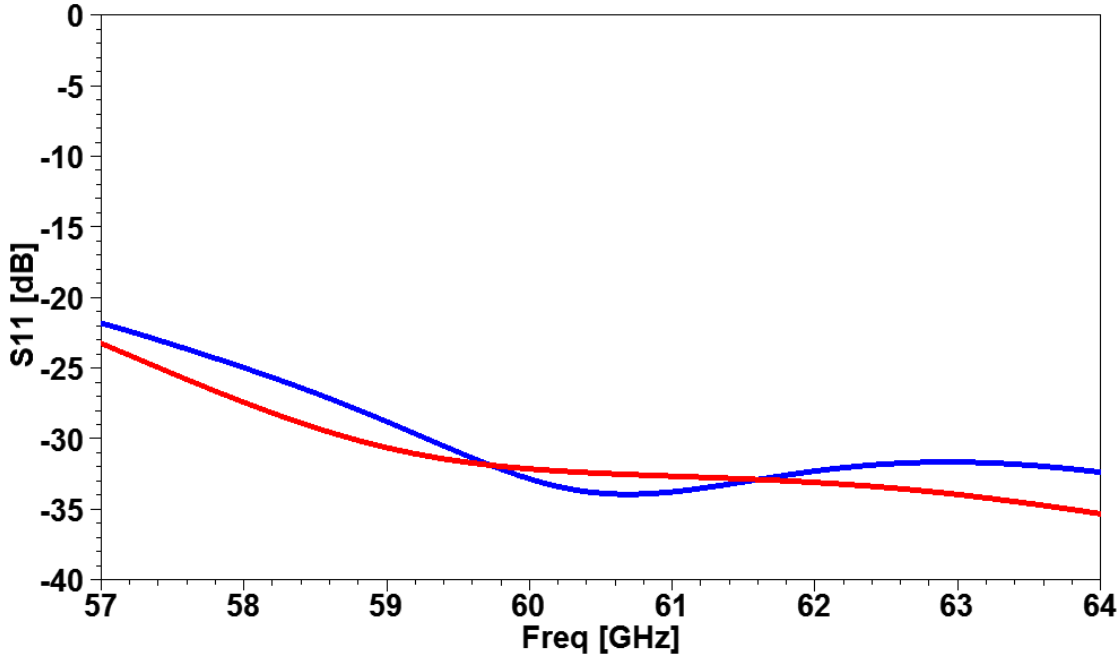

Fig. 3.3.1.2. Reflection coefficient for the fed with a dielectric-filled waveguide (red) and with SIW (blue).

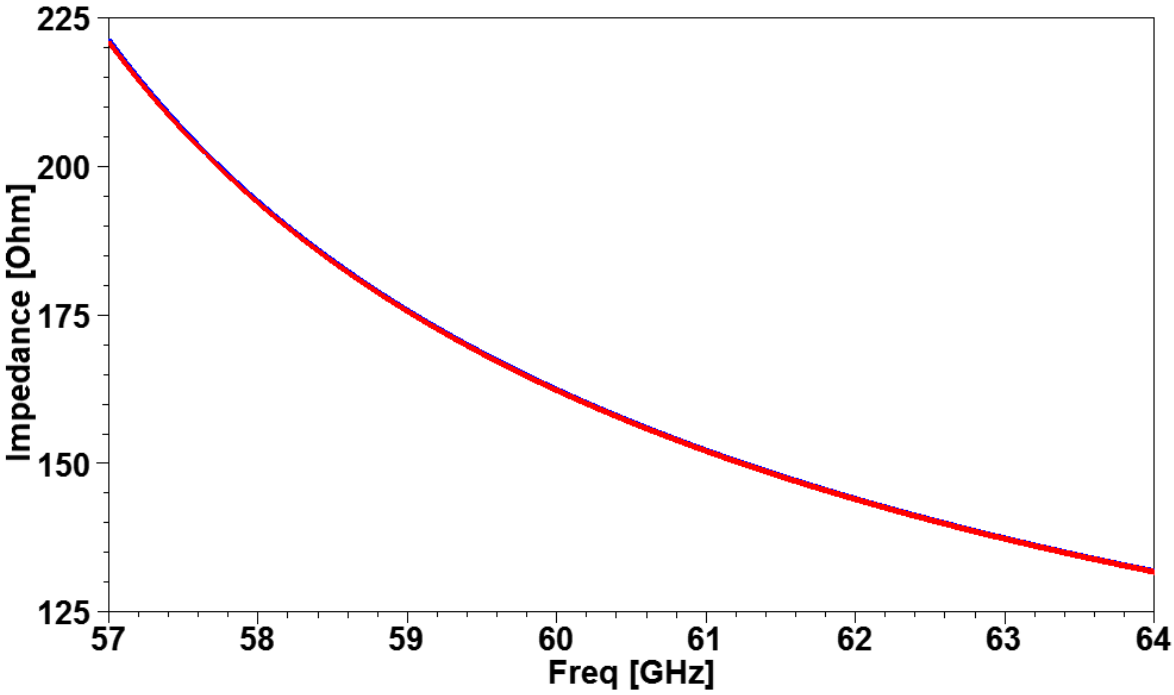

Fig. 3.3.1.3. Port impedance at the position for the H-slot aperture to the single element antenna.

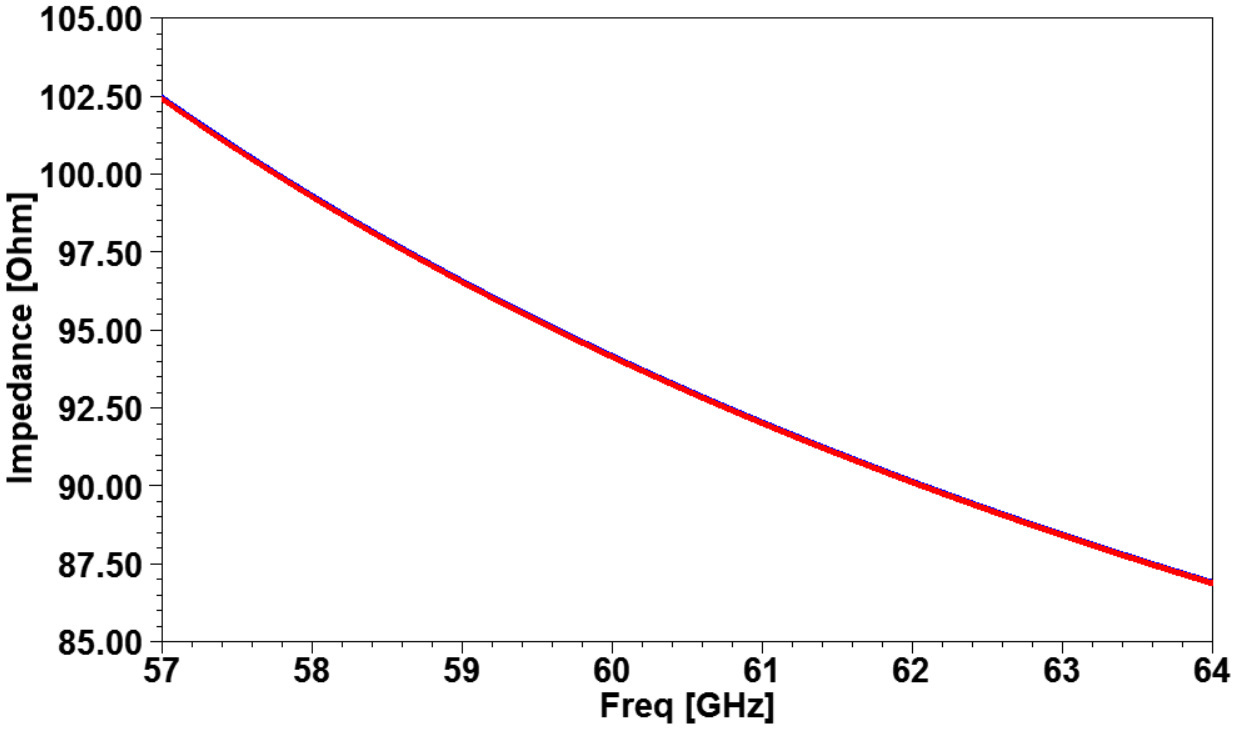

Fig. 3.3.1.4. Port impedance at the H-slot aperture to the coaxial transition.

3.3.2 2x2 Array Antenna Feed Phase Delay Transition

To feed the 2x2 array presented in sections 3.1.4 and section 3.2.3, a feed line with phase delay was design between two elements. The circularly polarized single element patches designed have high input impedance around 200 Ω to 220 Ω. Considering a T-power divider the impedance of the antenna will be reduce to a half of its original impedance. To incorporate the feed is necessary consider the current magnitude and the phase delay between the antenna apertures. Fig. 3.3.2.1 shows the design structure for the phase delay using filled-substrate waveguide with a power divider with a $\lambda_g/4$ transformer to match the line.

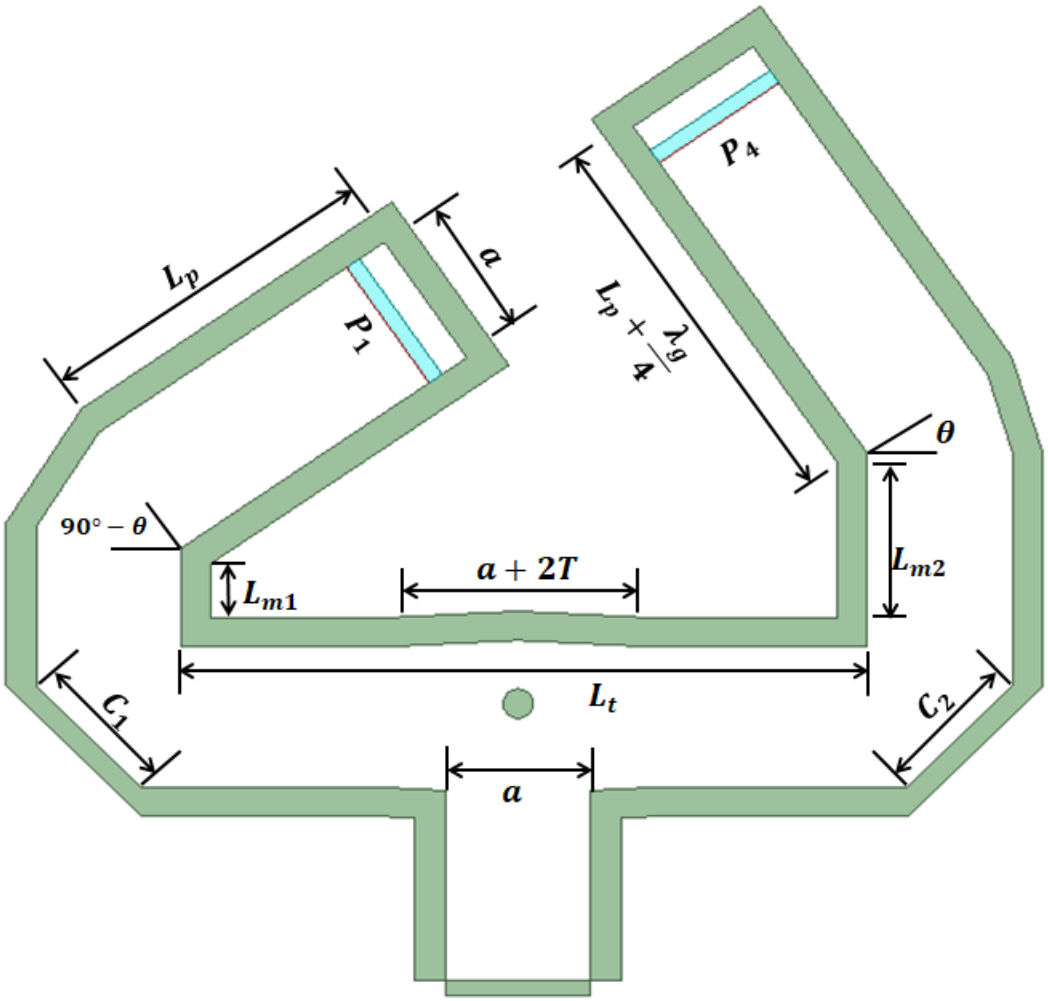

Fig. 3.3.2.1. Feed phase delay transition for two elements from 2x2 array antenna. The parameters are summarized in Table 3.3.2.1.

TABLE 3.3.2.1. Feed Phase Delay Parameters.

Parameter	Value	Parameter	Value
a	1.45mm	T	0.5034mm
L_p	3.4568mm	L_t	6.84mm
θ	26.52°	L_{m2}	1.6065mm
C_1	1.4849mm	L_{m1}	0.5692mm
C_2	1.4849mm	λ_g	2.6135mm

In order to implement the T power divider into the schematic the angles and lengths of the middle lines between the antenna line and the T power divider must depends on the real distance L_t. The length of L_{m1} can be determine by,

$$L_{m1} = L_{m2} - \sqrt{\left(L_p - \frac{a}{2} - L_s - 2r\right)^2 + \left(L_p - \frac{a}{2} - L_s\right)^2 - (L_t)^2} \qquad (3)$$

Where L_{m2} is fixed, a is the waveguide width, L_s is the distance between the H-slot and the short circuit wall, r is the radius of the vias, and L_t is varied.

The angle of the middle lines can be determine by,

$$\theta = \tan^{-1}\left(\frac{L_t}{\sqrt{\left(L_p - \frac{a}{2} - L_s - 2r\right)^2 + \left(L_p - \frac{a}{2} - L_s\right)^2 - L_t^2}}\right) - \phi \qquad (4)$$

Where ϕ is the angle of the triangle used to estimate the length of L_{m1} using L_{m2} as base variating the length of L_t. ϕ is determine by,

$$\phi = \tan^{-1}\left(\frac{\left(L_p - \frac{a}{2} - L_s\right)}{\left(L_p - \frac{a}{2} - L_s - 2r\right)}\right) \qquad (5)$$

In order to perform a delay line, one line length has a quarter lengths longer than the other, while both sides of the design have same magnitude with respect to the input. The design was done only for the filled-dielectric waveguide. Fig. 3.3.2.2 shows the reflection coefficient, and note that it is less than -15 dB in the band of interest. Fig. 3.3.1.3 shows the phase delay between waveport. The phase delay were approximate to $90°$ phase between port 1 (P_1) and port 4 (P_4). The feeding waveport position is to implement a next layer using another phase delay with the other two ports (P_2 and P_3) using H-slot apertures.

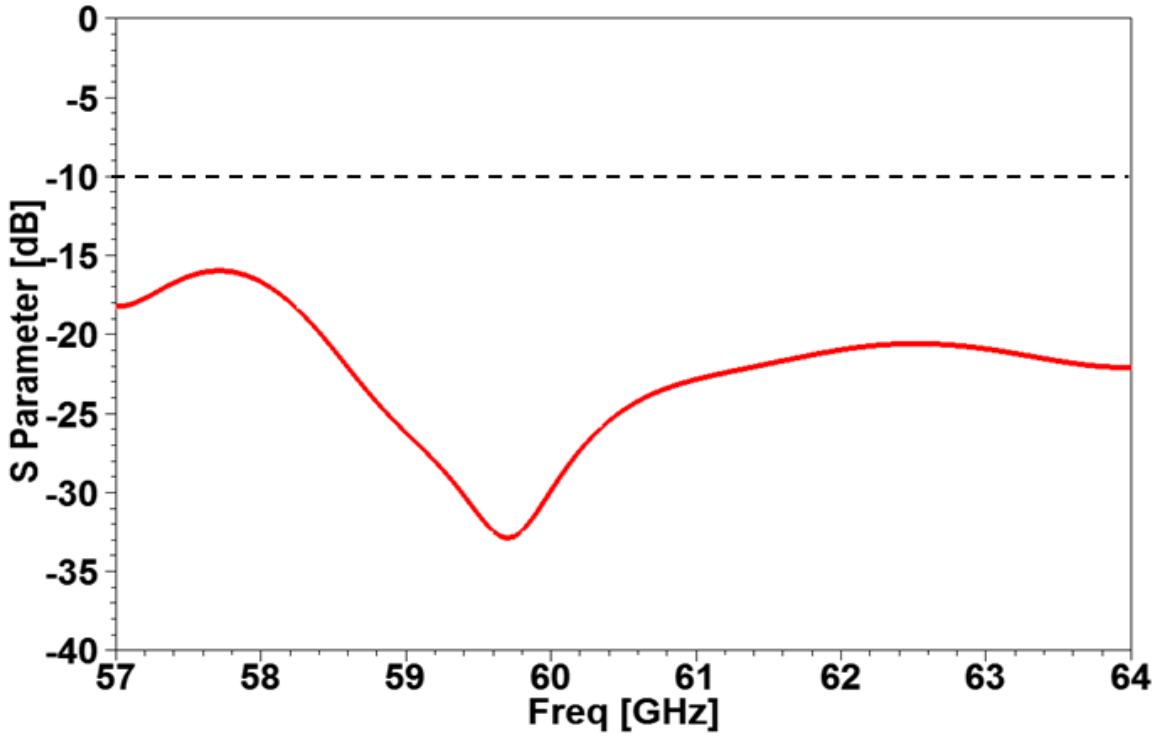

Fig. 3.3.2.2. Reflection coefficient first level 2x2 array antenna filled-substrate waveguide.

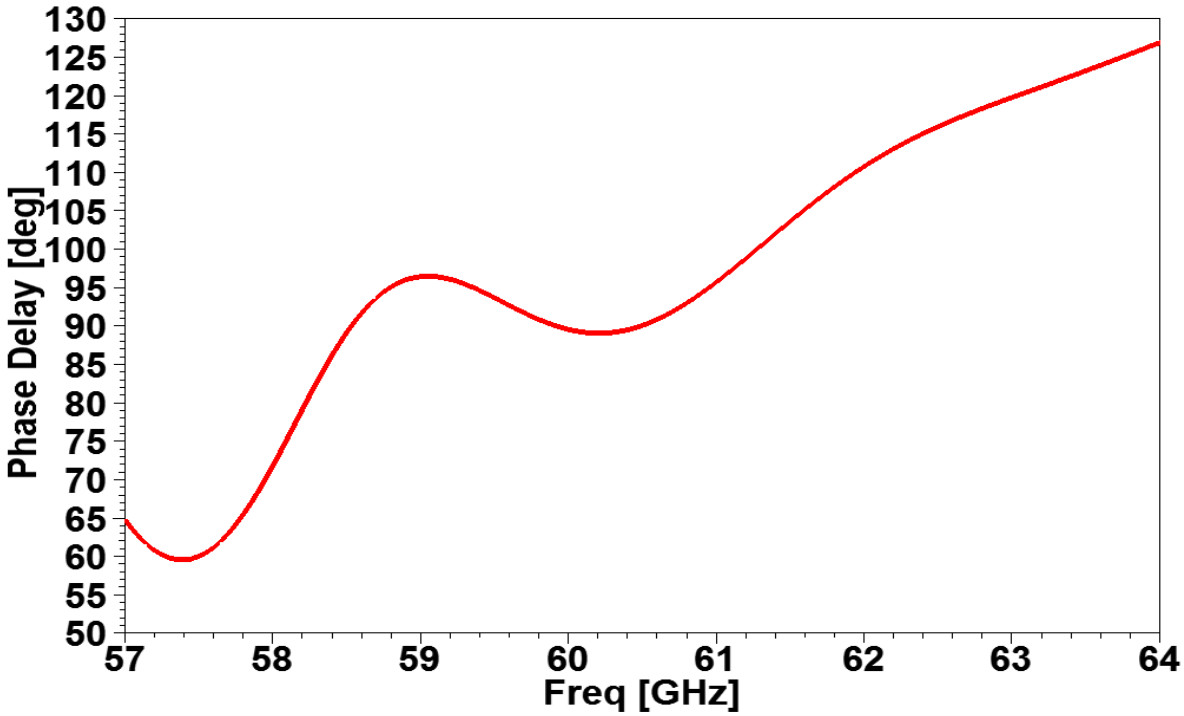

Fig. 3.3.2.3. Phase delay between ports of the 2x2 array antenna.

3.4 Coaxial Transition

To measure the designed antennas, a transition between coaxial and SIW was created. The coaxial transition works for both cases: single radiating element and 2x2 array. The model presented is using a SIW, but the analysis is valid for a dielectric-filled waveguide fed also. The impedance of the antenna must be reduced to match a coaxial port feeding the antenna. In the case of the array, the coaxial to SIW transition is used on the last power dividers in which the impedance will be reduced to that of a quarter of the impedance of the element. Fig. 3.4.1. shows the coaxial transition and the coaxial transition parameters values are summarized in Table 3.4.1.

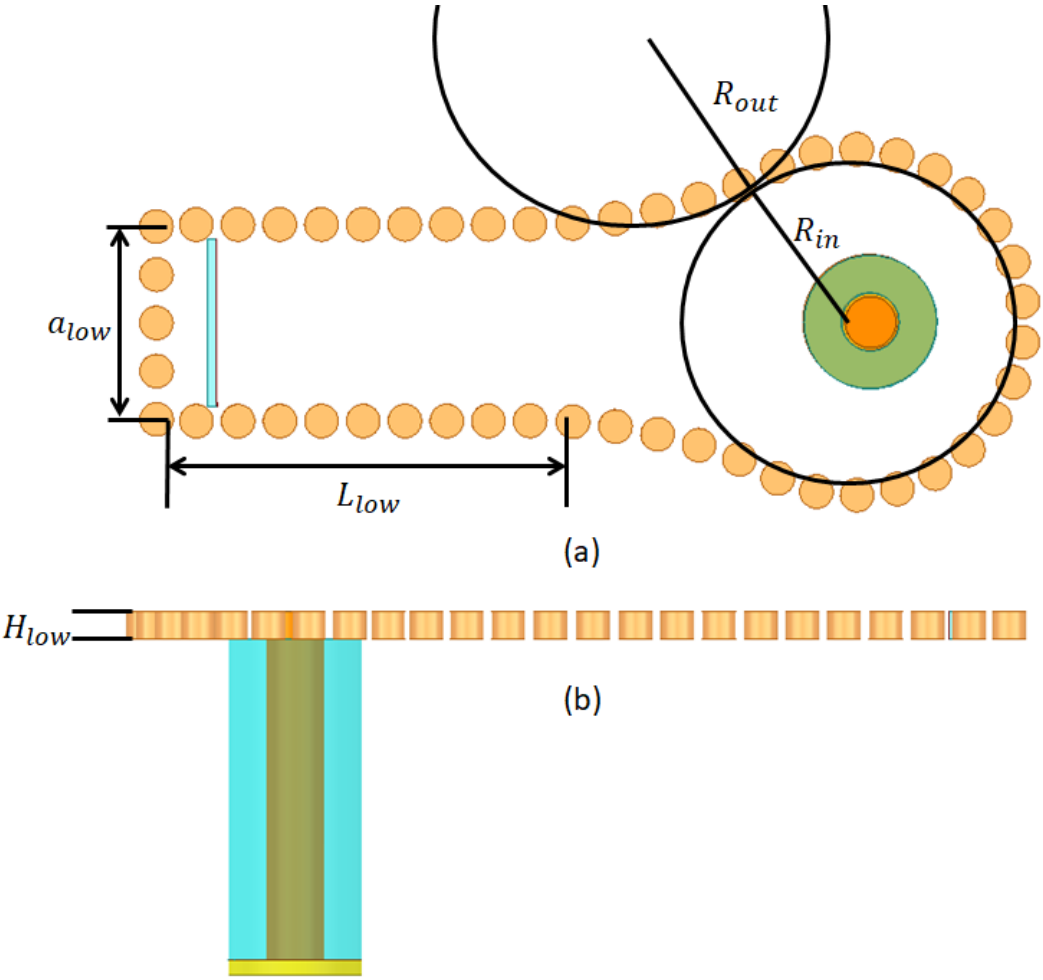

Fig. 3.4.1. Coaxial transition from $a_{eff} = 1.5mm$. (a) Top view model for the design SIW. (b) Side view model. The parameters shown are summarized in Table 3.4.1.

TABLE 3.4.1. Coaxial Transition Parameters.

Parameters	Value
a_{low}	1.72mm
R_{in}	1.4mm
R_{out}	5mm
L_{low}	5.63mm
H_{low}	0.254mm

To reduce the impedance of the line from 84 Ω to 50 Ω a tear drop was designed using three circles. The a_{low} part of the design has a characteristic impedance of 84 Ω, while the port has a characteristic impedance of 50 Ω. To match the SIW to the coaxial, the circles radius R_{out}, and R_{in}, were varied, as well the coaxial connector location. The coaxial offset from the center of the R_{in} circle is 0.12 mm to the wall. The coaxial connector used is a 1.85 mm connector.

Fig. 3.4.2 shows the reflection coefficient, where the reflection coefficient is less than $-15\ dB$ in the band of interest. Figs. 3.4.3 and 3.4.4, show the impedance for both ports against frequency. The impedance of the antenna at the SIW level is about 83 Ω, while the port impedance still center in 50 Ω. The wave-port is located at the middle of the H-slot aperture to couple into the SIW transition. The separation for the a_{low} wall to the port is of 0.43 mm, and it is used to reduce the reactance of the antenna directly to that point.

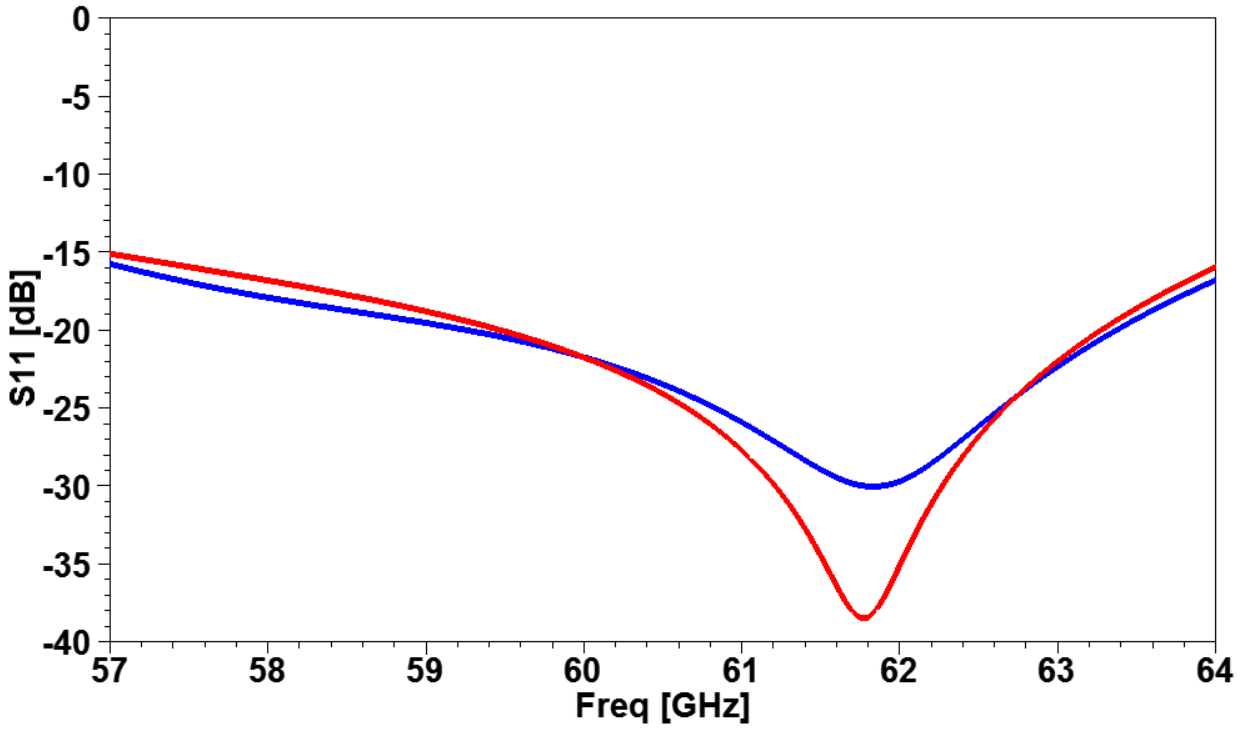

Fig. 3.4.2. Reflection coefficient for the coaxial transition fed with dielectric-filled waveguide (red) and with SIW (blue).

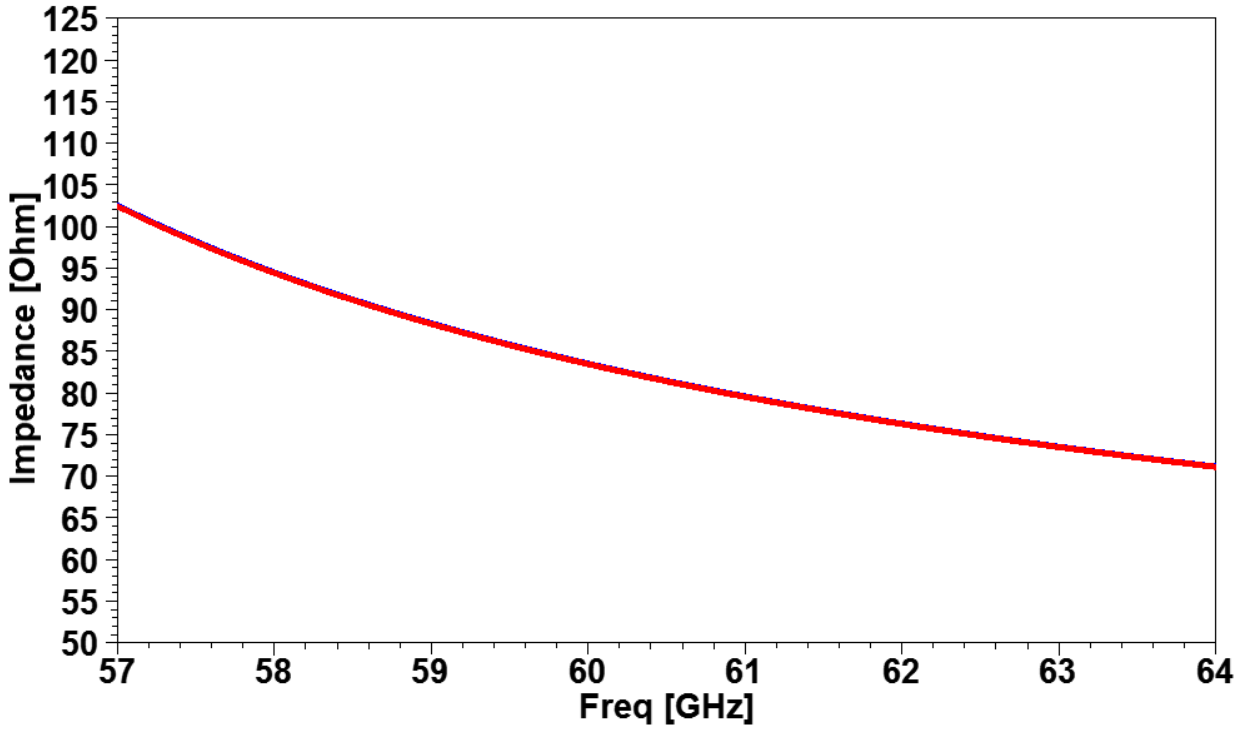

Fig. 3.4.3. Port impedance at the $a_{eff} = 1.5mm$.

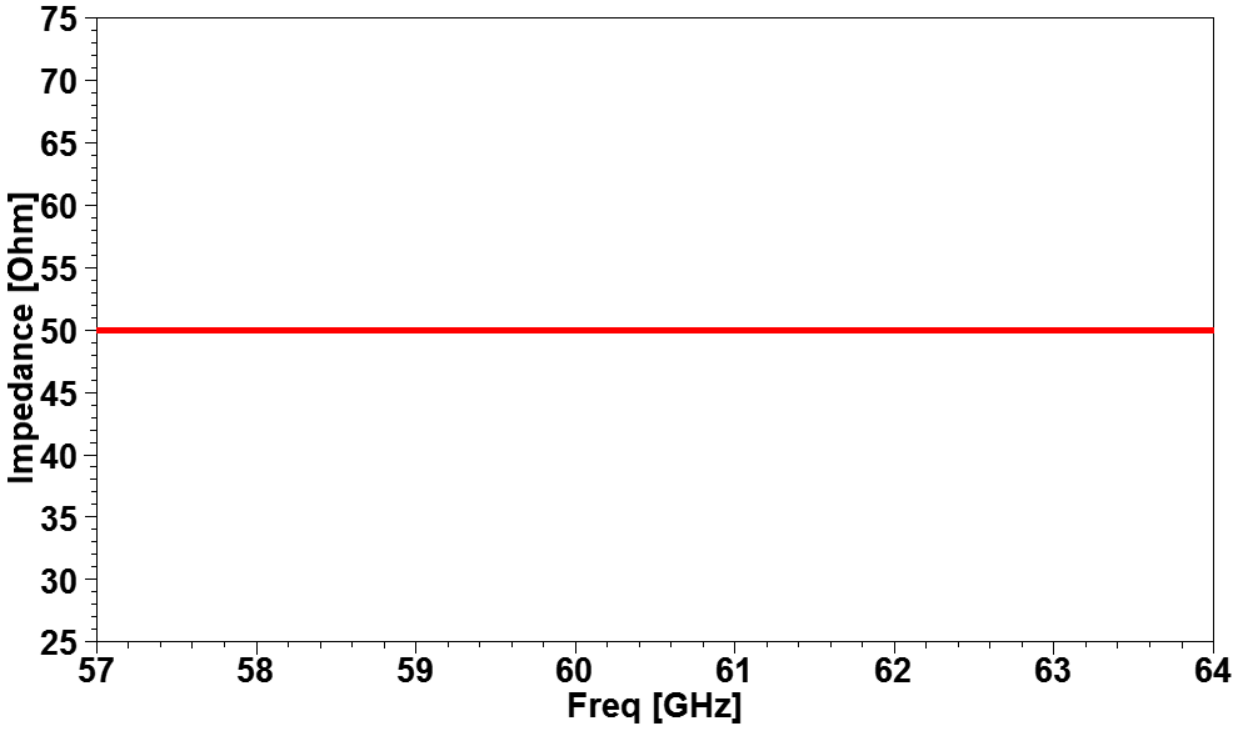

Fig. 3.4.4. Port impedance at the coaxial.

3.5 Human Body Modeling

The antenna model from [12] was used for human body tissue Design of Experiment to characterize the antenna parameters affected in presence of skin. The experiment fulfilled simulations similar to the research from [15] in which the antenna was conducted within V-band antenna. The study consists on developing equations describing dependence results of the antenna with respect of a design factor.

A 2^k factorial design with 3 parameters was conducted to determine which of the factors affect the electrical parameters of the antenna. The parameters used were HFSS solution frequency, antenna type (single element or array), and presence or absence of skin. The output observed were reflection coefficient, gain and the front-to-back ratio. Fig. 3.5.1. shows the factors and responses conducted for each of the experiments.

Std	Run	Factor 1 A:Solution Fr... GHz	Factor 2 B:Antenna T...	Factor 3 C:Presence ...	Response 1 Bandwidth GHz	Response 2 Gain dB	Response 3 FB ratio dB
1	2	60.48	Single	No	8.64	3.617	15.7107
2	6	65	Single	No	8.64	3.6114	15.7611
3	5	60.48	Array	No	8.64	15.419	17.8856
4	3	65	Array	No	8.64	15.482	17.6844
5	1	60.48	Single	Yes	8.64	3.3914	31.0048
6	8	65	Single	Yes	8.64	3.3889	30.6952
7	4	60.48	Array	Yes	8.64	12.358	17.5559
8	7	65	Array	Yes	8.64	14.171	24.2702

Fig. 3.5.1. Response data for each experimental case.

The experiment helped to determine that the bandwidth was not affected in the frequencies of interest; the FB ratio is strongly dependent on the presence of skin and the interaction of the antenna type with presence of skin; and the measured gain is dependent on the antenna type. All the results were expected from the beginning, but the most important factor is the presence of skin which only affect the FB ratio results. The antenna design from [12] has the same SIW fed idea from coaxial to the radiating elements.

CHAPTER 4

RESULTS

4.1.1 Single Element with Feed

The antenna in section 3.3 was implemented with the transition feed to drop the antenna impedance, using the section 3.4 method, and then reduce the impedance of the SIW to coaxial port using the design from section 3.5. The SIW feed was integrated to the model using a macro algorithm shown in Appendix A. The single radiating element contains two of feed layers. The first layer has the transition feed using taper to reduce the single element impedance and the second layer has the coaxial to SIW transition. The separation between a_{in} wall and the H-slot aperture couple is used to couple the reactance from the antenna. The first layer has a larger height from the second, because of the limited range of the SIW. All the parameters from the design consider fabrication restrictions. Fig. 4.1.1.1. shows the model with the two implementations.

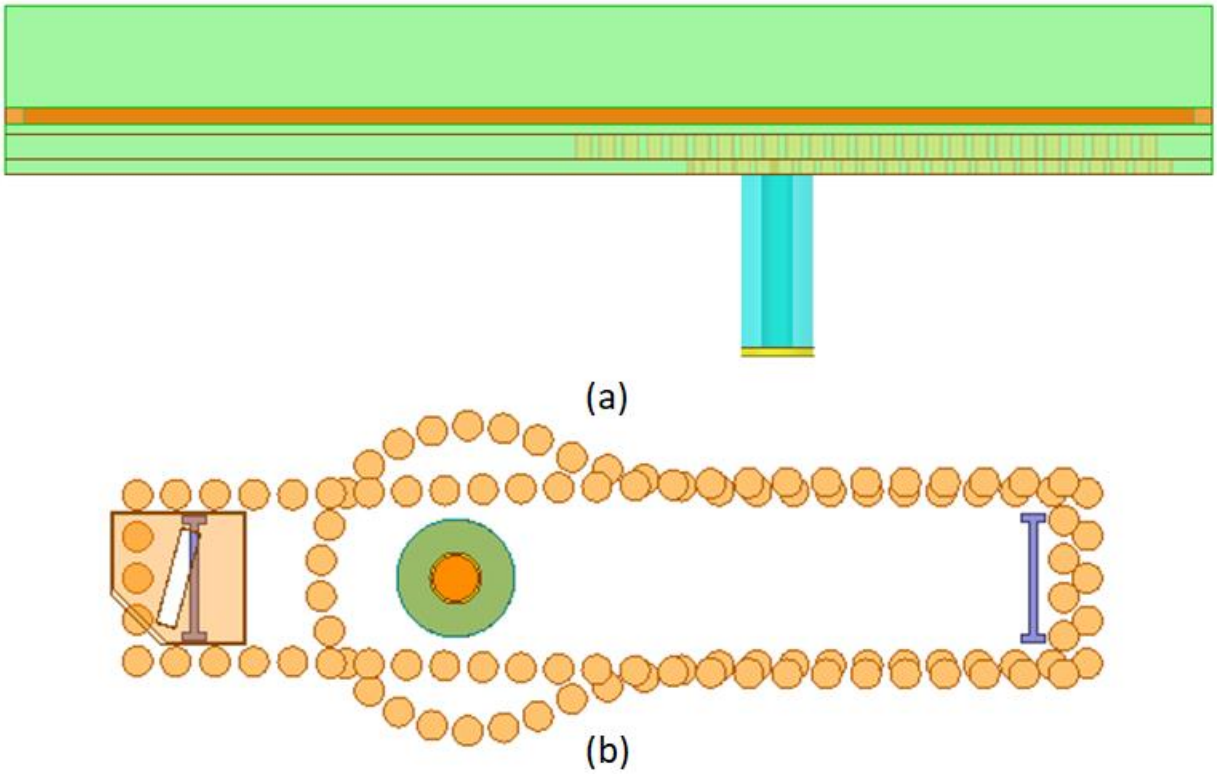

Fig. 4.1.1.1. Antenna design model. (a) Side view image. (b) Top view image.

Fig 4.1.1.2 shows the reflection coefficient covering the entire desire band with $S11 \geq -10dB$. The single element maintains its impedance bandwidth of 11.6%. Also, in Fig. 4.1.1.3 shows the smith chart of the antenna concluding that the final design has a 50 Ω resistance and no reactance. The axial ratio bandwidth is shown in Fig. 4.1.1.4. with a bandwidth of 8.7% from 58.1 GHz to 63.4 GHz. Fig. 4.1.1.5 shows the scanning capabilities, while keeping CP behavior, through the axial ratio. This design shows an axial ratio smaller than 3 dB $-7°$ to $8°$ in theta. This design has less beam steering capabilities that the single element from section 3.1.2. which has $66°$ power beamwidth. The CP gain is shown in Figs. 4.1.1.6., and 4.1.1.7. Fig. 4.1.1.6 shows the CP gain pattern and Fig. 4.1.1.7 the CP gain as a function of frequency. Note that the cross-polarization is -15.9 dB, and the co-polarization is 7.04 dB at 60 GHz. Fig. 4.1.1.8 shows the CP gain pattern at 60 GHz with sidelobes at $-26°$, and $27°$. Furthermore, in Fig. 4.1.1.9. shows the radiation efficiency. The antenna has losses due to the long used of the feed on substrate.

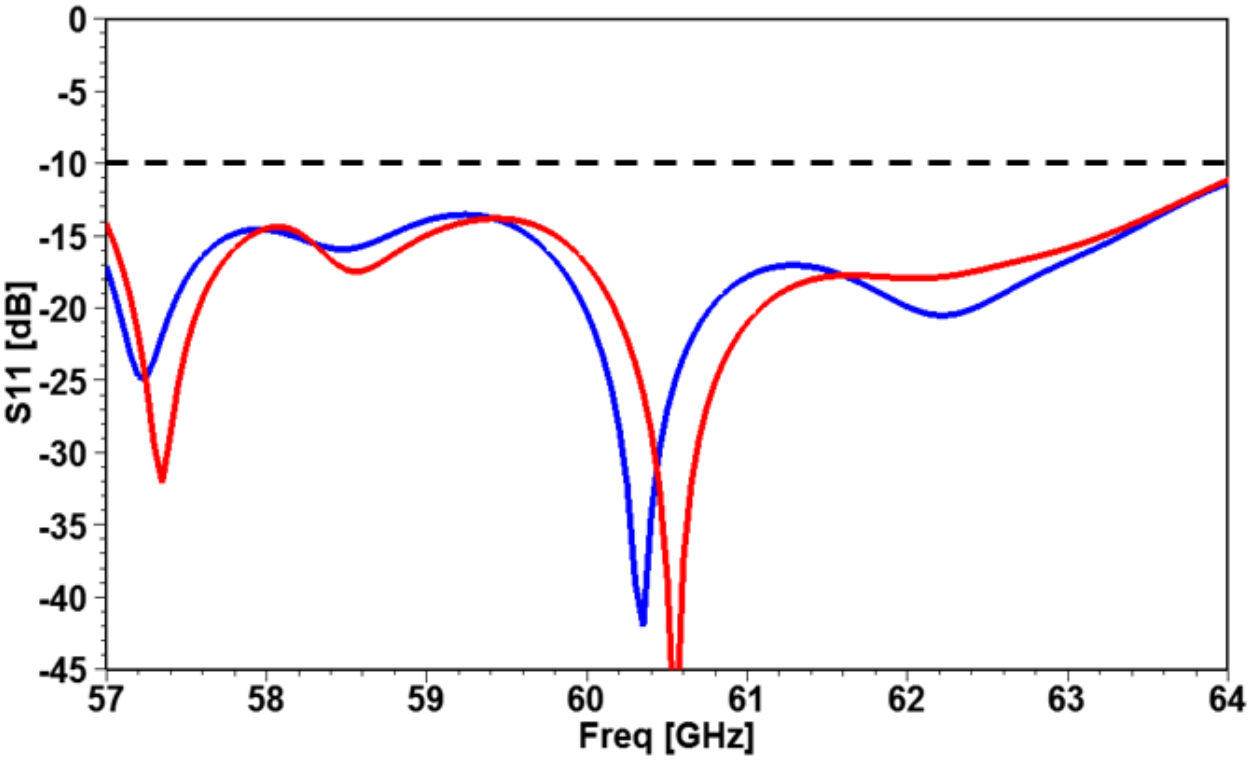

Fig. 4.1.1.2. Reflection coefficient for a single element fed with a dielectric-filled waveguide (red) and with SIW (blue).

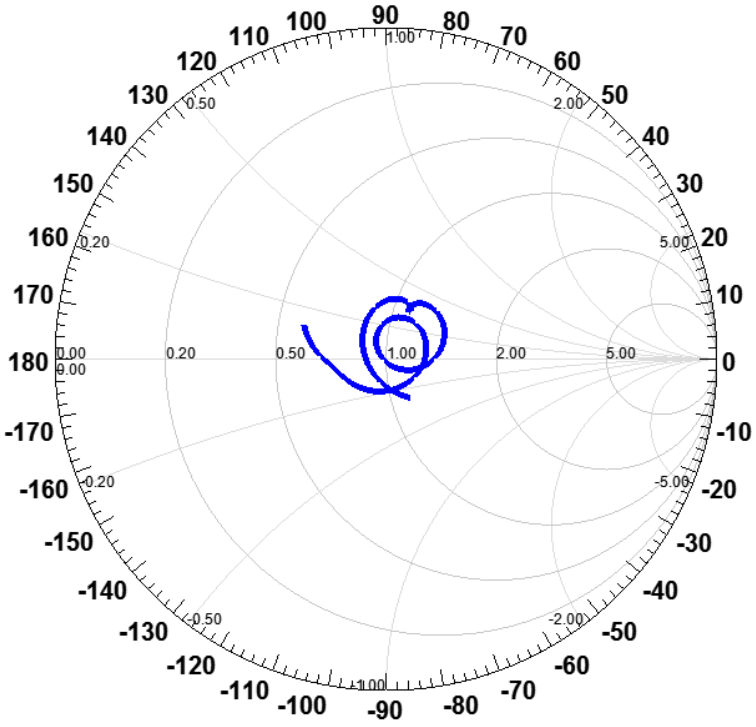

Fig. 4.1.1.3. Smith chart from the coaxial fed with SIW.

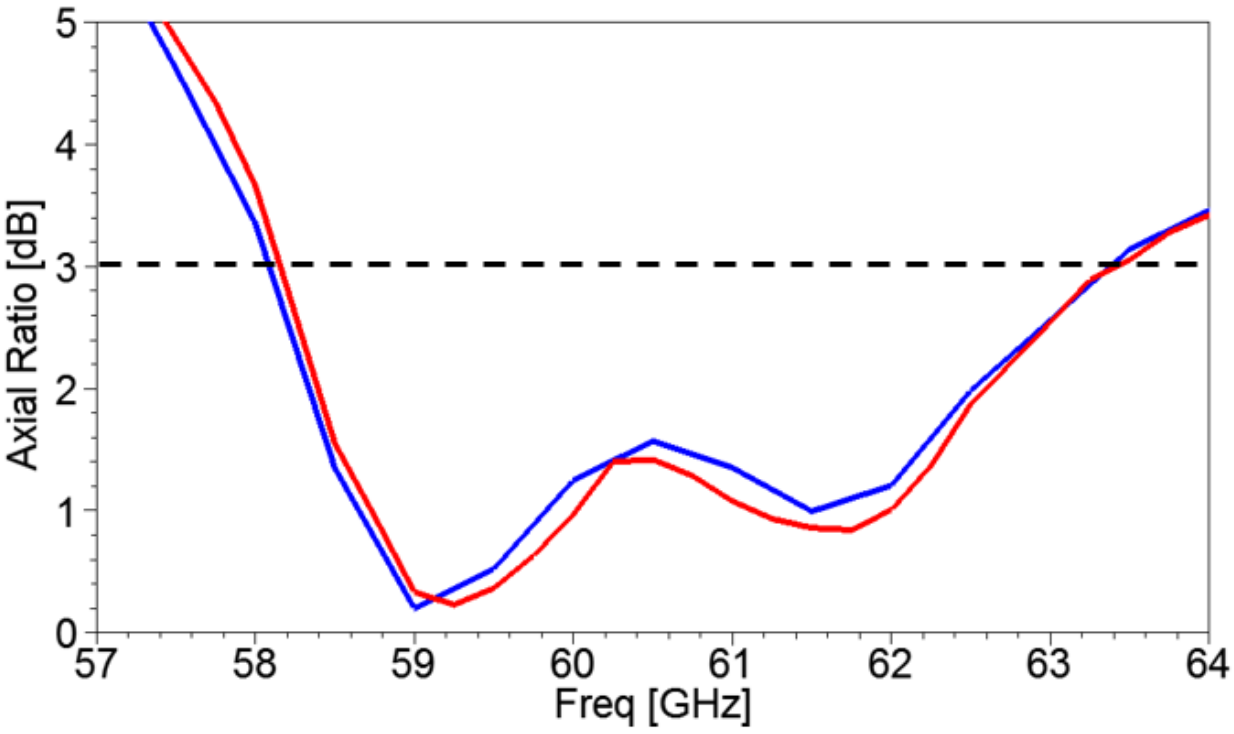

Fig. 4.1.1.4. Axial ratio bandwidth for a single element fed with a dielectric-filled waveguide (red) and with SIW (blue).

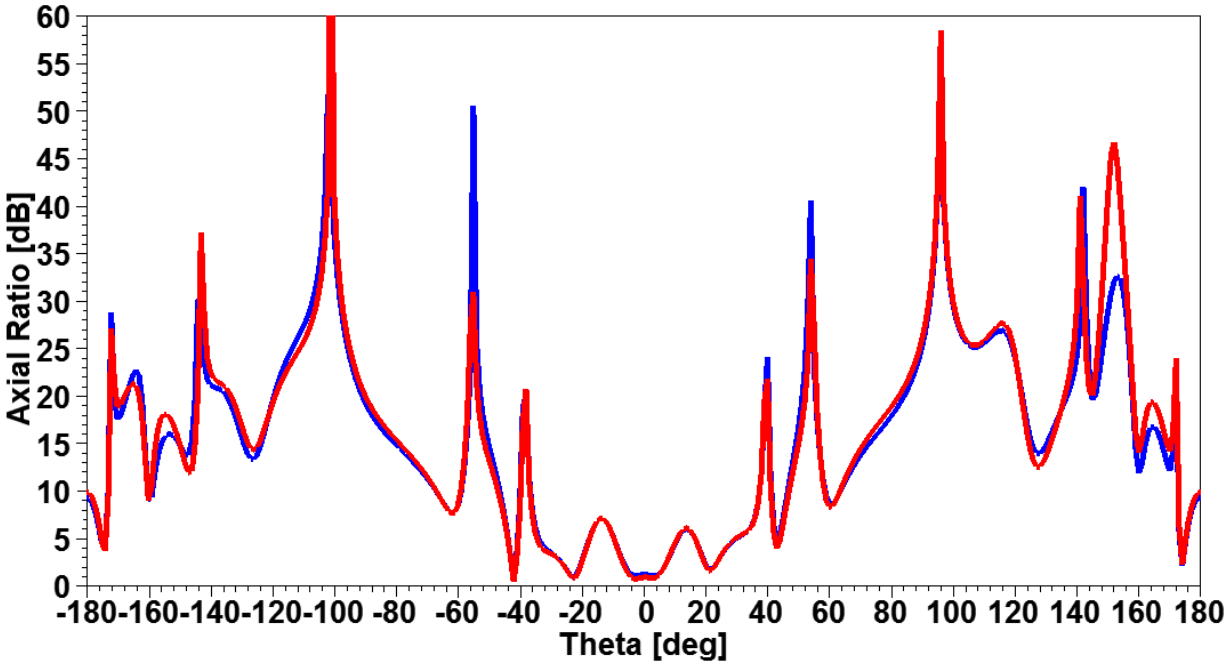

Fig. 4.1.1.5. Axial ratio as a function of theta at 60 GHz for a single element fed with a dielectric-filled waveguide (red) and with SIW (blue).

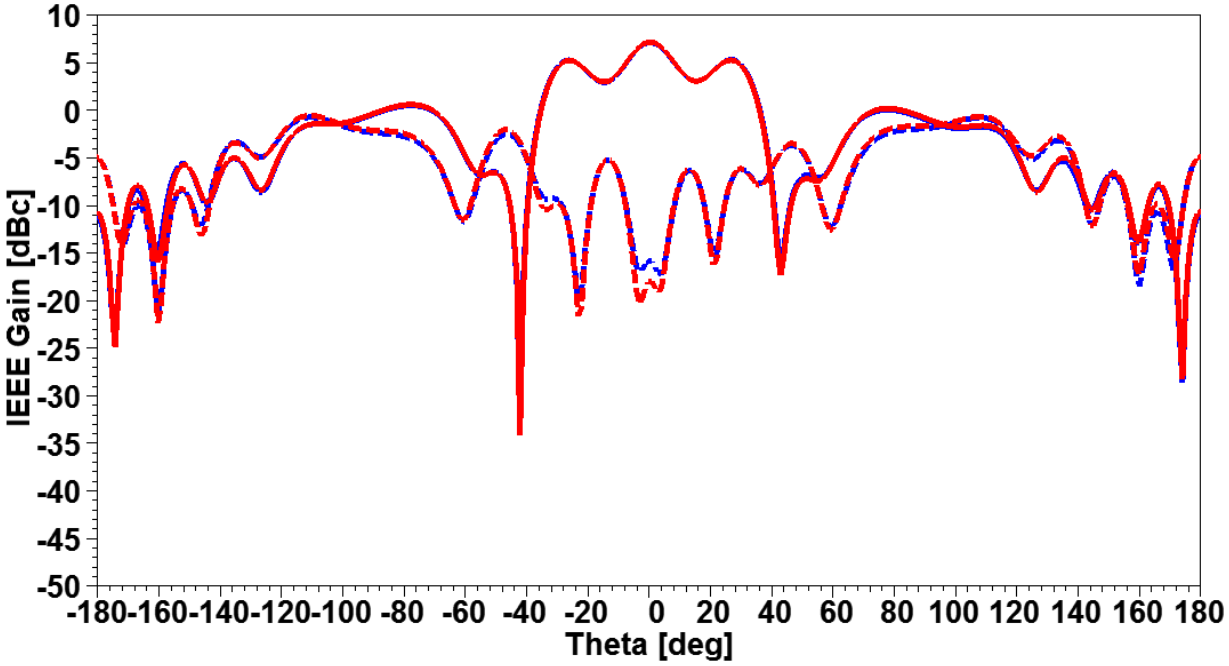

Fig. 4.1.1.6. CP gain pattern for a single element at 60 GHz fed with a dielectric-filled waveguide (red) and with SIW (blue). The dotted lines show the cross-polarized gain for the same cases.

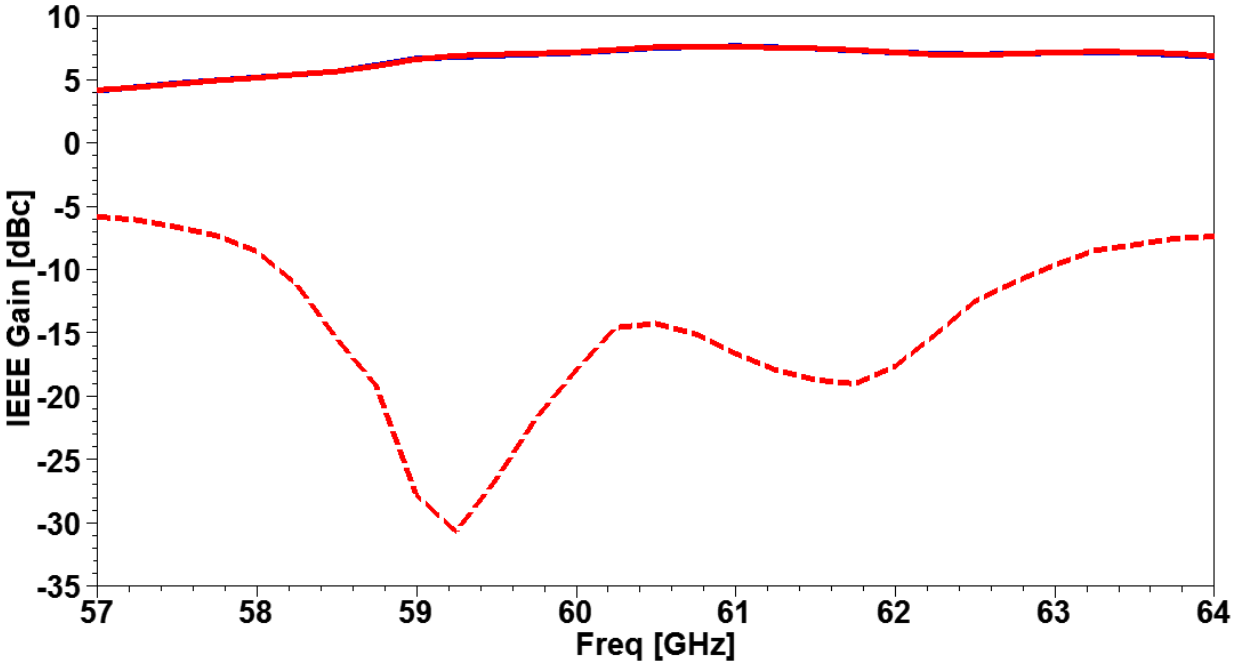

Fig. 4.1.1.7. CP gain for a single element fed with a dielectric-filled waveguide (red) and with SIW (blue). The dotted line show the cross-polarized gain for the same cases.

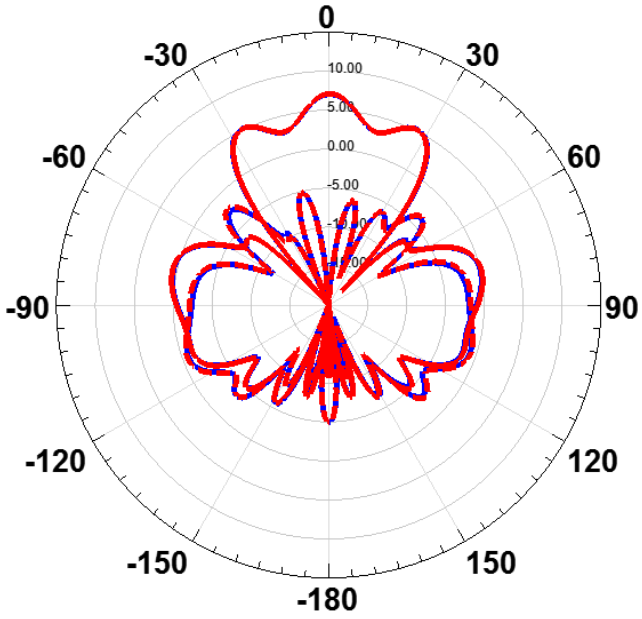

Fig. 4.1.1.8. CP gain pattern for a single element fed with a dielectric-filled waveguide (red) and with SIW (blue) at 60 GHz.

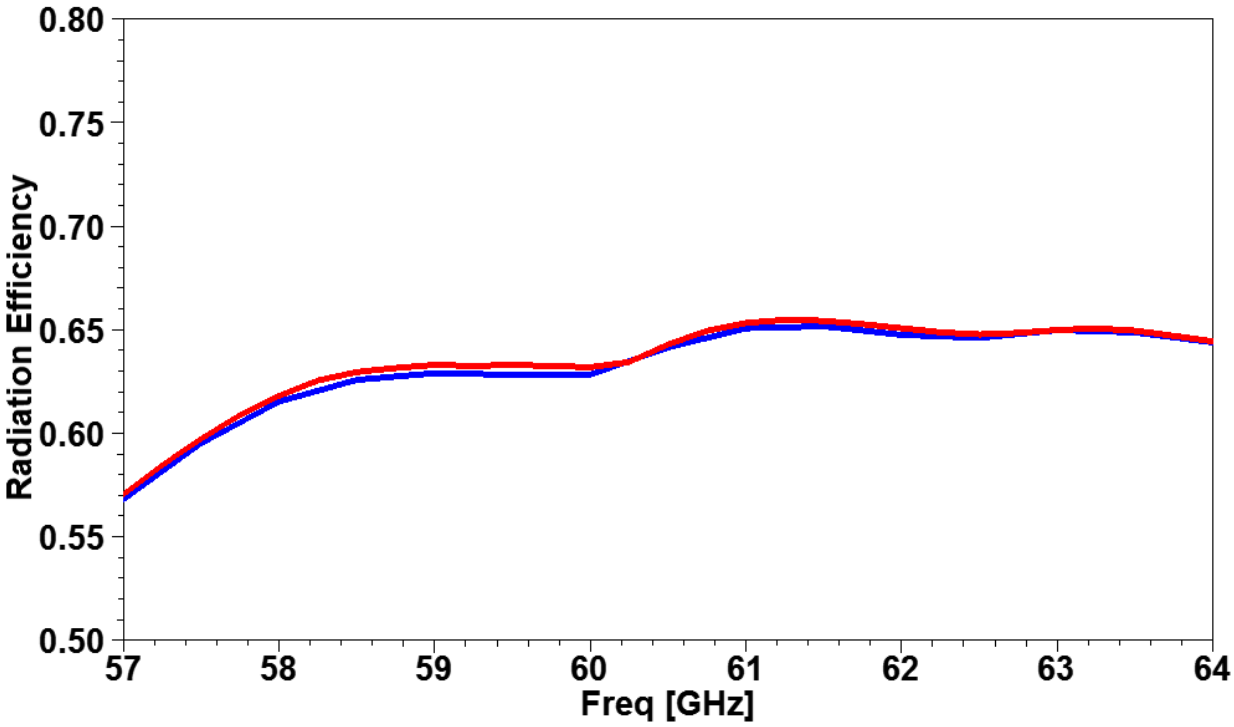

Fig. 4.1.1.9. Radiation efficiency as a function of frequency for the single element fed with a dielectric-filled waveguide (red) and with SIW (blue).

4.1.2 Single Element with Feed Sensitivity Study

Before fabricating, a sensitivity study was performed to determine the parameters would be affected by the tolerances by the manufacturer. The manufacturer offer $\pm 20.32 \mu m$ error tolerance for etching copper surfaces. The sensitivity study was performed using the etching on the aperture size as mismatch and etching error, while the patches has they own etching tolerance. In fig. 4.1.2.1 shows the reflection coefficient for the four cases: the tolerance on patches, the tolerance on the aperture. On red is shown the original behavior of the antenna without any sensitivity study. Furthermore, the antenna shows no effect on the reflection coefficient due to the fabrication limitations. Meanwhile, in fig 4.1.2.2 shows the axial ratio bandwidth for the previous cases. The fig shows that the size of the radiating element affects the axial ratio bandwidth. To reduce the fabrication error is needed less tolerance on the patch fabrication to reduce the effect in the axial ratio bandwidth for a single element.

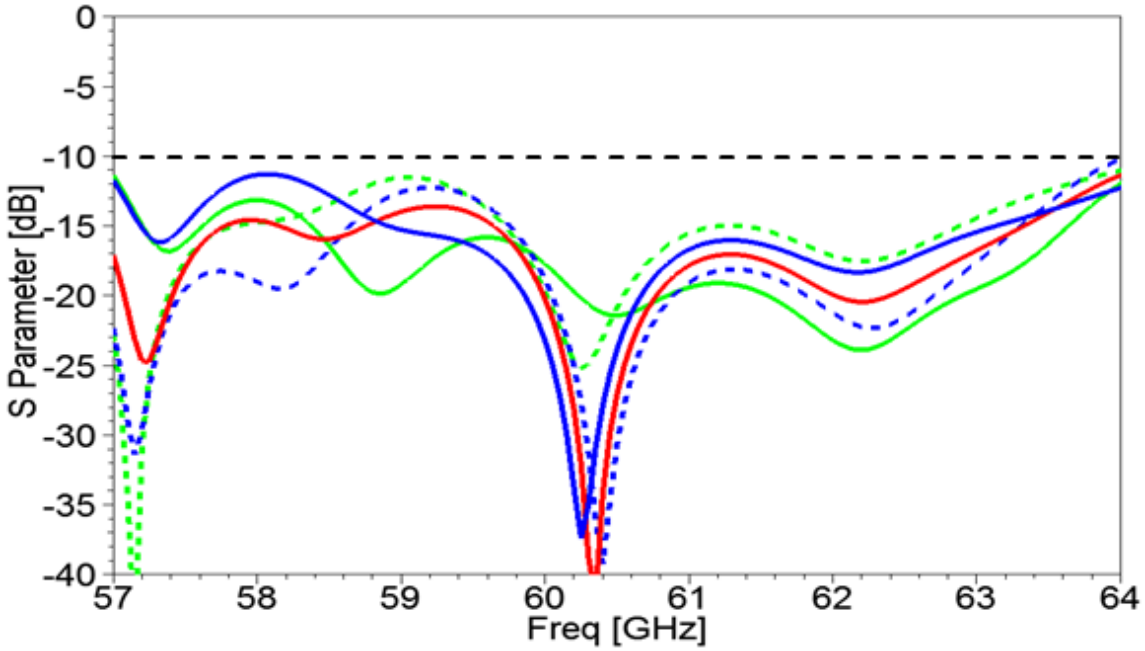

Fig. 4.1.2.1. Reflection coefficient for the variation on coupling aperture (green), antenna size (blue), and the original curve (red).

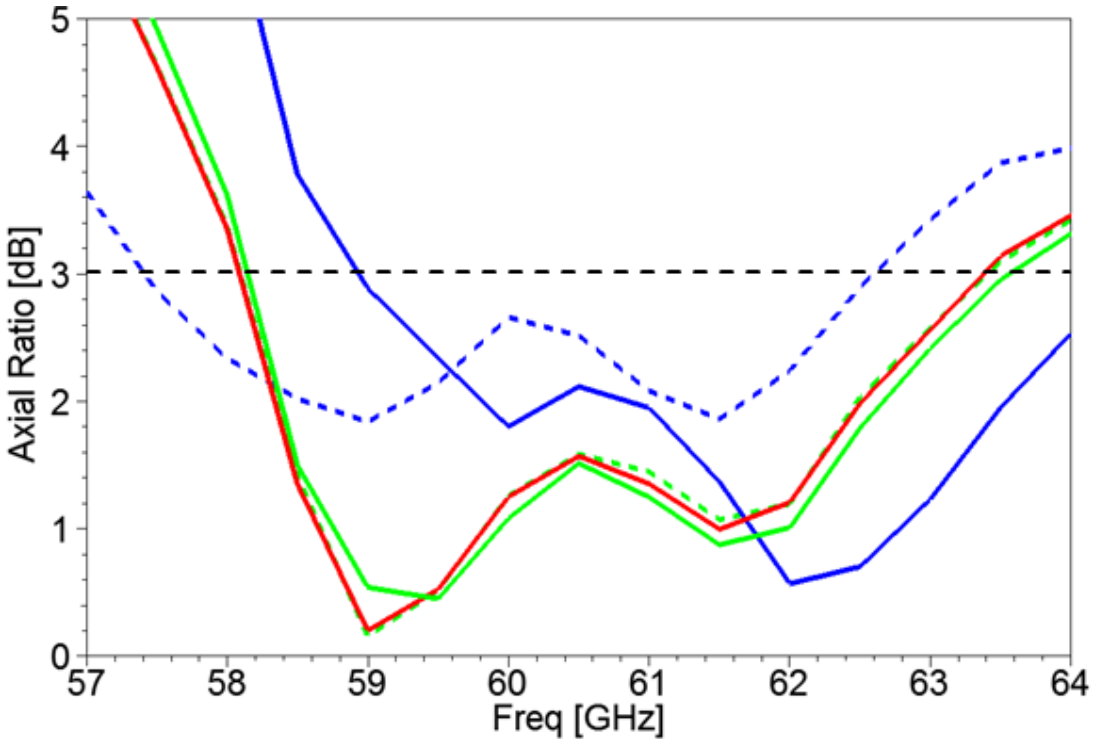

Fig. 4.1.2.2. Reflection coefficient for the variation on coupling aperture (green), antenna size (blue), and the original curve (red).

CHAPTER 5

CONCLUSION AND SUGGESTIONS FOR FUTURE WORK

This work shows a single element and 2x2 array antennas for body area network for off-body communications at 60 GHz. The single element achieves the impedance bandwidth and most of the axial ratio bandwidth requirements. On the other hand, the 2x2 array antenna achieves both completely, the impedance bandwidth and the axial ratio bandwidth. The single element improves the circular gain and is not affected when is implemented on an array using sequentially rotation. The feed for the single element was developed using taper to match the antenna to a coaxial transition. The transition method with wave-ports can be implemented to the 2x2 array. The transition helps to achieve the requirements without affecting the element parameters only affecting the CP gain cause of the SIW losses.

Human body design was developed in order to test the antennas radiation for use in body area network application. The antenna demonstrates independence to the presence of skin model in all the parameter except the front-to-back ratio. The FB ratio was expected to be affected due to the presence of skin absorb part of the radiation energy. The antenna performance will maintain its simulations pattern without the skin affecting the electrical parameters of the antenna.

5.1 Suggestions for Future Work

This work presented a fully functional antenna for BANs applications using circularly polarized at 60 GHz. The requirements were achieved with the single element and the 2x2 array. Also, were shown that the single element can be feed using SIW to coaxial. This feed can be implemented in the 2x2 array using power dividers on multi-layers. At the same time, the array propose in this work can be enlarged to reach more CP gain. In the future a characterization to know if there any effect on human skin tissue due to CP and array energy if is enlarged. Future work also should include a fabrication of the single element and 2x2 array, and measurement of both cases.

REFERENCES

[1] A. Pellegrini *et al*., "Antennas and Propagation for Body-Centric Wireless Communications at Millimeter-Wave Frequencies: A Review [Wireless Corner]," in *IEEE Antennas and Propagation Magazine*, vol. 55, no. 4, pp. 262-287, Aug. 2013.

[2] N. Chahat, M. Zhadobov and R. Sauleau, "Broadband Tissue-Equivalent Phantom for BAN Applications at Millimeter Waves," in *IEEE Transactions on Microwave Theory and Techniques*, vol. 60, no. 7, pp. 2259-2266, July 2012.

[3] R. Delgado, C. A. M. Hernández and R. R. Solís, "Applying design of experiments to the design of 60 GHz antennas for off-body communications," *2016 IEEE International Symposium on Antennas and Propagation (APSURSI)*, Fajardo, 2016, pp. 1641-1642.

[4] "An internet Resource for the Calculation of the Dielectric Properties of Body Tissues" Institute for Applied Physics, Italian National Research Council, http://niremf.ifac.cnr.it/tissprop.

[5] Steven Shichang Gao; Qi Luo; Fuguo Zhu, "Introduction to Circularly Polarized Antennas," in *Circularly Polarized Antennas* , 1, Wiley-IEEE Press, 2014, pp.328

[6] L. Sun, G. Ou, Y. Lu, and S. Tan, "Axial ratio bandwidth of a circularly polarized microstrip antenna," *Adv. Microstrip Antennas with Recent Appl.*, 2008.

[7] Y. Li, Z. N. Chen, X. Qing, Z. Zhang, J. Xu and Z. Feng, "Axial Ratio Bandwidth Enhancement of 60-GHz Substrate Integrated Waveguide-Fed Circularly Polarized LTCC Antenna Array," in *IEEE Transactions on Antennas and Propagation*, vol. 60, no. 10, pp. 4619-4626, Oct. 2012.

[8] Wong, K.L. and T.W. Chiou. Broadband single-patch circularly polarized microstrip antenna with dual capacitively coupled feeds, IEEE Trans. Antennas Propagat., 49(1):41–44, 2001.

[9] J. Huang, "A technique for an array to generate circular polarization with linearly polarized elements," in *IEEE Transactions on Antennas and Propagation*, vol. 34, no. 9, pp. 1113-1124, Sep 1986.

[10] K. S. Chin, W. Jiang, W. Che, C. C. Chang and H. Jin, "Wideband LTCC 60-GHz Antenna Array With a Dual-Resonant Slot and Patch Structure," in *IEEE Transactions on Antennas and Propagation*, vol. 62, no. 1, pp. 174-182, Jan. 2014.

[11] G. Kumar, and K. P. Ray, "Multilayer Broadband MSAs", in "Broadband Microstrip Antennas", 1st ed. Norwood, MA, Artech House, Inc., 2003, ch. 4, sec. 4.2.2, pp. 138-145.

[12] C. A. M. Hernandez and R. A. R. Solís, "Design of V-band SIW fed cavity backed aperture coupled microstrip patch array element for applications in body area networks," *2016 IEEE International Symposium on Antennas and Propagation (APSURSI)*, Fajardo, 2016, pp. 1235-1236.

[13] M. Bozzi, A. Georgiadis and K. Wu, "Review of substrate-integrated waveguide circuits and antennas," in *IET Microwaves, Antennas & Propagation*, vol. 5, no. 8, pp. 909-920, June 6 2011.

[14] Clyburn, Rosenworcel, and Pai, (2013, August 9), "Federal Communications Commission", (FCC 13-112), [Online] Available: https://apps.fcc.gov/edocs_public/attachmatch/FCC-13-112A1_Rcd.pdf

[15] N. Chahat, M. Zhadobov, L. Le Coq, S. I. Alekseev and R. Sauleau, "Characterization of the Interactions Between a 60-GHz Antenna and the Human Body in an Off-Body Scenario," in *IEEE Transactions on Antennas and Propagation*, vol. 60, no. 12, pp. 5958-5965, Dec. 2012.

APPENDIX A

```
import sys

sys.path.insert(0,'./grad_libs')

import utils

import hfss_siw

import siw

import waveguide

import simple_math

reload(utils)

reload(hfss_siw)

reload(siw)

reload(simple_math)

utils.setup(oDesktop,"Aperture_To_Antenna_Waveguide_SIW")

design_scope = {}

utils.setupEvaluableStrings(utils.oDesign,design_scope)

utils.setupUnitsAndConverter(design_scope,

                write_back_length_unit = 'mm',

                unit_length = "meters", unit_angle="deg")

nbaseCS = 'nbaseCS'

utils.setWCS('First_Layer_SIW_Init')

utils.createRelativeCS(origin = utils.ZERO_VECTOR, pointX = utils.UNIT_NX, pointY = utils.UNIT_NY, name =
nbaseCS)

cap1 = hfss_siw.SiwCap(name="cap1",

            baseCS = "nbaseCS",

            cap_type = 'OUT',

            clip = False,

            eff_width="a_waveguide_in",
```

```
                height="Hms",
                epsilon_r="epsilon_r",
                via_radius="via_radius",
                design_scope=design_scope,
                density=1)
siw1 = hfss_siw.SIW(name="siwin1",
                baseCS="First_Layer_SIW_Init",
                eff_length="Element_SIW_Length",
                p1_type="OUT",
                p2_type="EXACT",
                eff_width="a_waveguide_in",
                height="Hms",
                epsilon_r="epsilon_r",
                via_radius="via_radius",
                design_scope=design_scope,
                density=1,
                a_output_var = 'siw1_a',
                p1_clip=True,
                p2_clip=False)
siw2 = hfss_siw.SIW(name="taper",
                baseCS=siw1.endCS,
                eff_length="Feed_Lenght_Taper",
                p1_type="EXACT",
                p2_type="EXACT",
                wg_param_pack = siw1.generate_wg_param_pack(),
                eff_width_p1 = siw1.eff_width,
                eff_width_p2 = "a_waveguide",
                a_output_var = 'siw1_a1',
```

```
                p1_clip=True,
                p2_clip=True)
siw3 = hfss_siw.SIW(name="siwout2",
                baseCS=siw2.endCS,
                eff_length="Feed_Lenght_Out+Wap+Ls1",
                p1_type="EXACT",
                p2_type="OUT",
                wg_param_pack = siw2.generate_wg_param_pack(),
                eff_width= siw2.eff_width_p2,
                a_output_var = 'siw1_a2',
                p1_clip=False,
                p2_clip=False)
cap2 = hfss_siw.SiwCap(name="cap2",
                  baseCS = siw3.endCS,
                  cap_type = 'OUT',
                  clip = True,
                  wg_param_pack = siw3.generate_wg_param_pack())
nSecondBaseCS = 'nSecondBaseCS'
utils.setWCS('Second_Layer_SIW_Init')
utils.createRelativeCS(origin = utils.ZERO_VECTOR, pointX = utils.UNIT_NX, pointY = utils.UNIT_NY, name =
nSecondBaseCS)
cap3 = hfss_siw.SiwCap(name="cap3",
                  baseCS = "nSecondBaseCS",
                  cap_type = 'OUT',
                  clip = False,
                  eff_width="a_waveguide_lower",
                  height="Hms1",
                  epsilon_r="epsilon_r",
```

```
                via_radius="via_radius",
                design_scope=design_scope,
                density=1)
siw4 = hfss_siw.SIW(name="siwlow1",
                baseCS="Second_Layer_SIW_Init",
                eff_length="Cavity_Cilinder_x_center-X_radios+Wap+Ls2",
                p1_type="OUT",
                p2_type="EXACT",
                wg_param_pack = cap3.generate_wg_param_pack(),
                eff_width= cap3.eff_width,
                height="Hms1",
                epsilon_r="epsilon_r",
                via_radius="via_radius",
                design_scope=design_scope,
                density=1,
                a_output_var = 'siw1_a3',
                p1_clip=True,
                p2_clip=False)
tear1 = hfss_siw.SiwTearDropTransition(name = 'teardrop1',
                                baseCS = siw4.endCS,
                                radius = 'Rcavityport',
                                bev_radius = 'Rcircle',
                                clip = True,
                                wg_param_pack = siw4.generate_wg_param_pack())
tear1.draw()
```